New types of synthetic periclase identified by C_2S inclusions - dicalcium silicate cement hardener

Adolf Peretti [1,2]*, Willy Bieri [1], Edward Cleveland [2], Matthias Alessandri [3], Stefan Kradolfer [4], Detlef Günther [4], Mario Meier [5], David Jaramillo [5] and Maya Musa [1]

[1] GRS Gemresearch Swisslab AG, Baumschulweg 13, 6045 Meggen, Switzerland / * corresponding author, e-mail: adolf@peretti.ch

[2] GRS (Thailand) Co., Ltd., Unit 501-506, Silom 19 Building, Soi 19, Silom, Bangrak, Bangkok 10500, Thailand

[3] GRS Lab (Hong Kong) Limited, 19/F, Man Hing Commercial Building, 79-83 Queen's Road Central, Hong Kong, China

[4] ETH Zurich - Hönggerberg, Laboratory of Inorganic Chemistry, Building HCI, Vladimir-Prelog-Weg 1-5/10, 8093 Zürich, Switzerland

[5] Particle Vision GmbH, c/o Fri Up, Annexe 2, Passage du Cardinal 11, 1700 Fribourg, Switzerland

Introduction

Naturally occurring periclase is a relatively common mineral phase. Due to its small crystal sizes, it never gained recognition in the gem-industry in terms of commercial importance. Synthetic periclase is commonly used for technological applications and is available in large quantities and sizes *(Joachin et al., 2012)*. In the past, synthetic periclase was marketed in the United States as "lavernite" *(Liddicoat, 1969)*. Concerns about the stability of synthetic periclase have been reported (transforming into brucite with time and exposure) in previous publications *(Brown, 1993)*.

Green synthetic periclase was described in 1996 in the gem-market *(De Maggio, et al., 1997)*. In 2018, a series of faceted and rough gemstones of different colors were submitted to GRS, including brownish-orange, colorless, yellow and green stones. The material was offered as natural garnet, presumably originating from Turkey. The owners submitted a video supposedly of the mine with scenes portraying active hammering on what appeared to be a marble rock *(Fig. 1)*, including dolomite marbles. However, natural periclase is actually very rare and almost never found as big crystals in nature, while synthetic periclase is widely produced for various technical applications.

De Maggio et al. (1997) and Brown (1993) report that synthetic periclase is a manufactured in Australia from refractory magnesia for the purpose of producing a new synthetic product. They describe the process as follows: The process uses magnesite nodules (magnesium carbonate) from the Kunwarara deposit near Rockhampton in Queensland (Australia), which are crushed and heated to produce calcinated magnesia. The material can then be electro-fused to form ingots of fused synthetic periclase. Rings of periclase with different structure and sizes are formed *(Brown, 1993)* and also pseudo-cubic masses bounded by cleavage planes. The material reported by De Maggio, et al. (1997) was identical to our samples. The rough material contained the typical interlocking large crystals *(Fig. 2a.)*.

For our research, more than 24 samples were available *(Fig. 3)*. Two of the submitted faceted stones were accompanied by gemlab reports. One laboratory located in the JTC building *(Jewelry Trade Center)* in Bangkok, stated "Natural Grossularite (-Hessonite-Garnet)" for the brown material and the orange material was identified as "Natural Grossularite (-Andradite-Garnet)", indicated as "Mali"-Garnet. An additional report *(No. 2307565776)* by GIA states "periclase" but correctly indicates that *"the natural or synthetic origin of this stone cannot currently be determined"*.

Due to these discrepancies in identifying the material, GRS laboratory was contacted to further investigate the sample. The identification was important because large volumes of rough were available in the market and investors were willing to acquire the goods in larger quantities.

Additional information was provided by the seller of this new material that included a technical report from a "High-tech University Facility" with X-ray diffraction data confirming the material as being "periclase" as well as details about the formation of this material as a product of a natural geological processes in dolomite marbles. The report was accompanied by a mining movie *(see Fig. 1)*.

We were given the permission to crush some of the rough material for the purpose of targeting various types of inclusions. It turned out to be the only way of successfully solving the question about the identity of the material being of natural or synthetic origin. Furthermore, a series of high-tech instruments were necessary, such as available at the GRS laboratories in Bangkok, Hong Kong and Switzerland, as well as at specialized laboratories of Prof. Detlef Günther at the ETH Zurich and a private SEM-laboratory in Fribourg, both in Switzerland.

Figure 1a-d. Screen-shots of the movie that the supplier provided as "proof" of authenticity. The video shows a rock suite that looks like a dolomite marble outcrop, where he hammered a piece off the rock and produced a sample that resembles the material available. However, large deposits of natural periclase do not exist in nature and it would not be feasible to recover stones from an outcrop with such little effort. It was no surprise to learn that the material is actually synthetic and that the presented footage was fabricated.

Figure 2a. A selection of rough synthetic periclase (larger piece 10cm in length), with cm-large clear and facetable domains. Note the distinct cleavage in different directions and the interlocking crystals. **Figure 2b. (inlay)** A selection of synthetic periclase ranging from 5 to 10 cts of different colors (in GRS collection). In 2018, these samples were presented as a new type of natural gemstone in the Bangkok market.

Figure 3. A selection of rough and faceted samples of different colored synthetic periclase (yellowish-green, yellow, orange-brown and colorless) representative of what appeared in the market in Bangkok.

Material and Methods

Conventional gemological tests

The gemological characteristics of four selected samples obtained by conventional testing procedures are summarized in table 1.

SEM analysis

In order to obtain morphological details at high magnification and resolution, as well as to visualize differences in the chemical composition of the stones and the chemical characterization of the inclusions, SEM-EDS technique was applied on two selected rough samples. The samples were carbon coated and mounted on aluminum stubs prior to analysis at the Particle Vision GmbH laboratory in Fribourg, Switzerland.

A ZEISS Gemini 300 (FEG-SEM) equipped with a 4 quadrant, pneumatically retractable BSE detector and an EDS System consisting of an Oxford AZTec Advanced Microanalysis X-Max 80 mm2 EDS-detector (large window area for EDS analysis in low kV reaching nanometer-scale resolution and detection of low z elements) and the AZTec Software was used.

Quantification of carbon and oxygen must be regarded as qualitative due to difficulty in quantification of low z elements. Carbon is detected in the EDS spectra, but it was not quantified due to carbon coating interfering with the signal from the sample. In general, the quantification presented here must be regarded with care as the analyses were not performed on polished surfaces. However, semi-quantitative data was produced, the presence of different chemical elements was analyzed and element distributions were determined.

Highly magnified images were acquired with a BSE detector for purpose of visualizing compositional contrast. All images and SEM-EDS chemical element signals were acquired at an accelerating voltage of 12 kV for improved spatial resolution (aperture 60 μm and 8.5 mm working distance). Complementary analyses were performed at 25 kV to separate overlapping peaks and missed peaks of heavier elements.

Raman analysis

The Raman analyses were performed at GRS Switzerland by the Renishaw InVia confocal micro-spectrometer, equipped with a Leica microscope (5x, 20x, 50x and 100x objects), 514.5 nm and 785 nm laser sources as well as a charge-coupled device air-cooled detector (CCD). The instrument calibration was carried out before each analysis section by checking the position and intensity of standard silicium band at 520.6 ± 0.1 cm^{-1}. The Raman analyses were applied to four samples in order to identify the gemstones on the basis of the Raman vibrational modes and to identify inclusions. Moreover, the same samples and inclusions analyzed by SEM were tested by Raman to obtain a positive identification using chemical and structural controls.

Photoluminescence analysis

The photoluminescence analysis were performed at GRS Thailand using the GemmoRaman-532SG, equipped with a 532 nm laser source in connection with an external and thermoelectrically cooled CCD-type Ocean Optics QEPro spectrometer.

FTIR analysis

FTIR analyses were carried out at GRS Switzerland by a Spotlight 200i micro-ATR coupled with a Frontier FTIR spectrometer by Perkin Elmer. The analyses were performed in transmission mode and by ATR *(Attenuated Total Reflectance)* technique, in order to obtain absorption profiles of the bulk crystals as well as in the fingerprint spectroscopy area. To balance signal against noise, 256 cycles were performed for each analysis at $4cm^{-1}$ of resolution.

UV-Vis-NIR analysis

UV-Vis-NIR spectroscopy was applied in order to identify the characteristic absorptions of different colored synthetic periclase. We used a Lambda 950 spectrometer of Perkin Elmer at GRS Switzerland that is equipped with an integration sphere. The spectra were carried out in 250-860 nm range and at 1nm of resolution in scanning mode using a holographic grating and CCD detector (most of todays application use multichannel detectors). The system was used to avoid potential fluorescence interferences.

LA-ICP-MS analysis

Two samples of synthetic periclase with two different colors (green and orange) were measured with LA-ICP-MS *(results see table 2)*.

The following instrumentation was used: A GeoLas C (Coherent, ArF-excimer 193 nm) with an ablation frequency of 5 Hz, spot size 80 μm, laser energy 1.15 mJ, fluence 23 J/cm^2, coupled to a Element 2 sector field ICP-MS instrument (Thermo Fisher, Waltham, Massachusetts, USA), using dry argon plasma conditions, Al-cones, a dwell time of 0.01s. The measurements were made with approx. 40 s of the blank followed by approx. 40 s of signal acquisition from a single crater ablation.

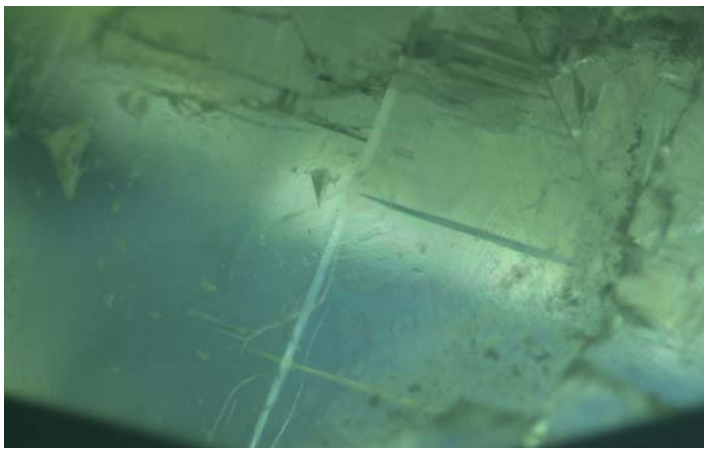

Figure 4. Synthetic green periclase reveals perpendicular cracks (photo micrograph).

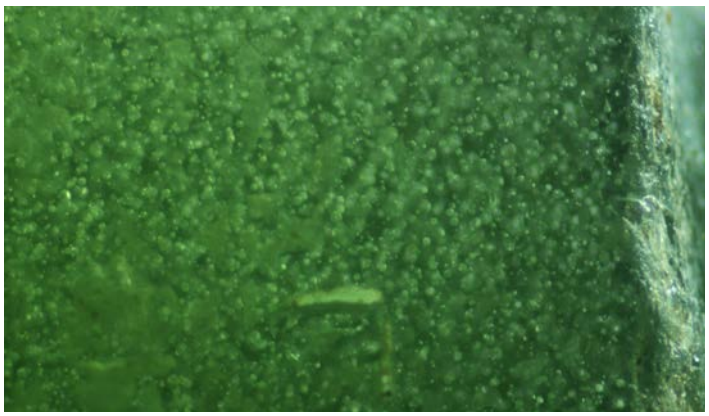

Figure 5. Inclusions as seen in green synthetic periclase. Some of the round inclusions are found to belong to the forsterite-monticellite series.

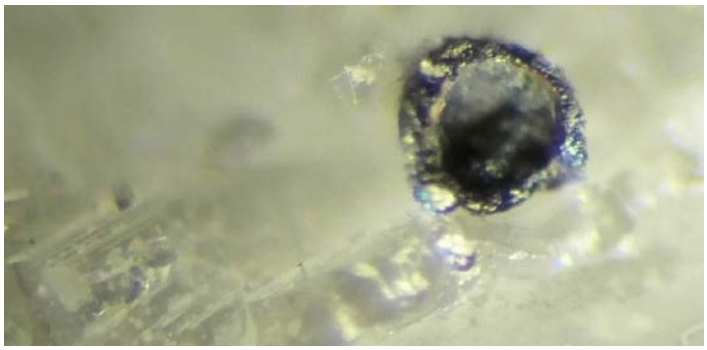

Figure 6. Close-up photo of synthetic C_2S (cement hardener) included within synthetic periclase (on the left). It has been found in the surrounding area of the black crystal. The inclusion reached the surface when a synthetic periclase was broken up. Surface analysis of this inclusion by SEM see Fig. 14b. The black material is a complicated phosphorous bearing substance high in carbon concentration. It is interpreted as a "rubber" slag (see Fig. 13a).

The major element Mg was used as an internal standard for the chemical analysis calculation, based on the chemical information obtained from EDS-SEM. The acquired signal was corrected against a preliminary measured background and internally corrected by the chosen internal standard. The quantification is based on the sensitivity given by an external calibration approach with a matrix matched standard and an additional 100% normalization.

DiamondView fluorescence

Fluorescent images were acquired on the four samples using the DiamondView IIDGR part of DeBeers Group Company instrument which is equipped with a 225 nm source.

Results

Gemological tests

Typical refractive indices's (R.I.) and densities were found that matched either grossularite or periclase. Specific gravity shows no difference between natural and synthetic periclase. No difference was found in the R.I. and S.G. between different color varieties *(Tab. 1)*.

No birefringence or anomalous double refringence was found for all colors (including colorless, not shown in table). Generally no fluorescence was observed in all the samples under long wave (LW) and short wave (SW) excitations, except for the green sample, which showed a faint yellow fluorescence under both UV-sources *(Tab.1)*.

The material was of high transparency and high crystallinity. The rough showed a clear distinct cleavage into two different perpendicular directions *(Fig.4)*. A variety of inclusions was found, such as shown in Fig. 5 and 6, including pin points, rounded crystals and fluid inclusions. Some of the inclusions were identified by SEM and Raman spectroscopy *(Fig. 20 and 21)*.

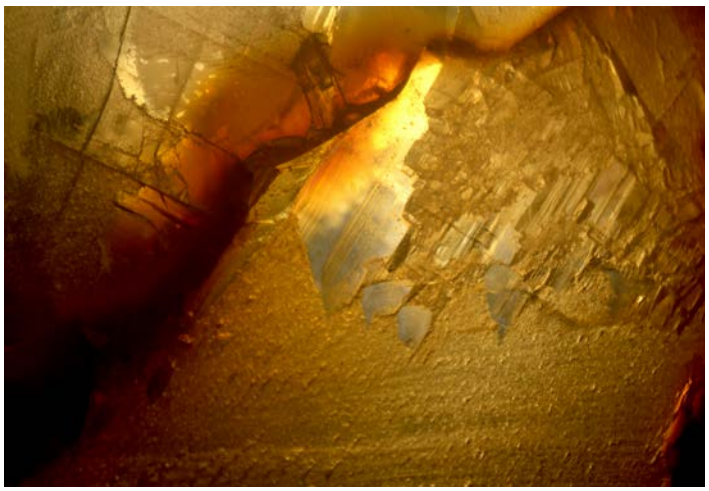

Figure 7a. This synthetic orange periclase shows a distinctive orange coloration at the contact of different domains of crystal growth (about 3 cm in diameter), indicating that circulating fluids along crystal domains introduced some trace elements for coloration of this synthetic product.

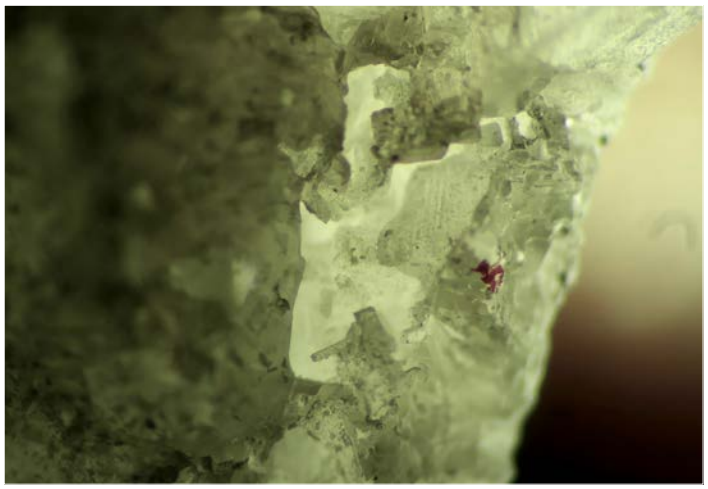

Figure 7b. Close-up photo of synthetic C_2S (cement hardener) that has been found in the surrounding area of the black crystal (whitish fissure network). The area was broken up from the center of a synthetic periclase. Surface analysis by SEM see Fig. 17a.

	SRef-060811	SRef-060812	SRef-060813	SRef-060814
Mineral identification	Synthetic Periclase	Synthetic Periclase	Synthetic Periclase	Synthetic Periclase
Carat weight	0.44 ct	0.22 ct	0.43 ct	1.99 ct
Shape & Cutting	Rough, partially polished	Rough, partially polished	Rough, partially polished	Rough, partially polished
Dimensions	6.28 x 4.79 x 1.93 mm	4.46 x 3.17 x 1.52 mm	6.32 x 3.17 x 1.52 mm	9.26 x 7.04 x 2.96 mm
Transparency	Transparent	Transparent	Transparent	Transparent
Color	Green	Polychrome, bi-color orange - colorless	Polychrome, bi-color yellow - colorless	Orange
R.I.	1.739	1.739	1.739	1.739
Birefringence	Absent	Absent	Absent	Absent
S.G.	3.59	3.59	3.59	3.59
Fluorescence	(LW) Faint yellow (SW) Faint yellow	(LW) None (SW) None	(LW) None (SW) None	(LW) None (SW) None

Table 1 Gemological properties of selected samples *(see Fig. 8.)*

Figure 8. A selection of the samples analysed in this study. The new generation of synthetic periclase presents a wide range of color varieties. The gemological properties are reported in table 1.

Spectroscopy

UV-VIS-NIR

The absorption spectra acquired by a UV-VIS-NIR spectrometer of the four samples are reported in Fig. 9. The green sample reveals more broad bands at about 440, 480, 520 and 610 nm, while the two bi-color samples show bands at 480 and 520 nm. The spectrum of the orange sample only shows a broad band at about 480 nm.

FTIR

The FTIR absorption spectra acquired using micro-ATR technique in transmission mode on the bulk crystals are reported in *Appendix B*. In all the samples are well visible very faint and broad bands at about 3300, 850 cm^{-1} and a strong band at about 603 cm^{-1}. Due to the application of a fitting software, a second band is also visible at about 645 cm^{-1}. The broad band at 3300 cm^{-1} in the OH-range is visible only on ATR spectra, while it disappears in the bulk analyses. In Joachin, et al. (2012) is reported that the synthetic periclase could present its characteristic visible double peaks at 3312 and 3297 cm^{-1}, but only after a hydrogenation process. The synthetic periclase is typically anhydrous. These peaks are absent in all the analyses performed. Moreover, no band correlated to brucite OH vibrational modes has been detected in our samples.

Although Farmer (1974) and Raman (1947) report very low absorption bands for MgO substance between 400 and 700 cm^{-1}, the same range where we registered the most intense fingerprint-band, a good band match result is difficult because of errors caused by the detector cut-off.

Raman

To improve the identification of gem materials, a micro-Raman characterization of the bulk crystals was carried out. The spectra are reported in *Appendix A*. When using a green laser source, strong fluorescence bands were registered in the higher region of the fingerprint spectroscopic range. Those bands disappear when using the 785 nm source, proving a fluorescence interpretation. Even though the MgO has no first order Raman scattering *(Farmer, 1974)*, faint broad bands around 480 and 600 cm^{-1} were registered. This fact could be correlated to the iron presence *(Marchetti et al., 2000)*, but other test must be done to improve the statistics. No OH-band has been registered in any sample *(see Appendix A)*. Several inclusions were characterized using a micro-Raman spectrometer. Gaseous inclusions, olivines *(Mohanan & Sharma, 1993)* and amorphous material *(Fig. 20-21)*.

In order to improve the inclusion characterization, the micro-Raman analyses were applied also on the inclusions revealed by BSD detector during the SEM-EDS study. Where the EDS micro-probe reveals the presence of iron, a hematite Raman spectrum has been obtained *(Fig. 16)*. Focusing the Raman source on the fibrous crystals observed by SEM and characterised by only Mg presence, any first order bands are not registered in the spectra *(Fig. 13e)*, as it is known for MgO crystals *(Farmer, 1974)*.

In all samples areas corresponding to a chemical composition characterised by Ca and Si, the Raman spectrum reveals bands as reported in figure 13c. Despite the similarity in the Ca and Si ratio between the chemical composition of these particles and the larnite mineral composition, the Raman bands of this mineral reported in the RRUFF database *(R070530)* are different. In fact, according to references *(Ibanez, et al., 2007; Ramirez & Carrasco, 2011)* that Raman spectrum is ascribable to synthetic Portland cement products, known as C_2S.

Finally, nano-crystals of carbonatic phases, calcite and aragonite, were detected associated to prismatic crystal inclusions *(Fig. 20a-b)*.

UV-Vis-NIR absorption spectroscopy of synthetic periclase of different colors

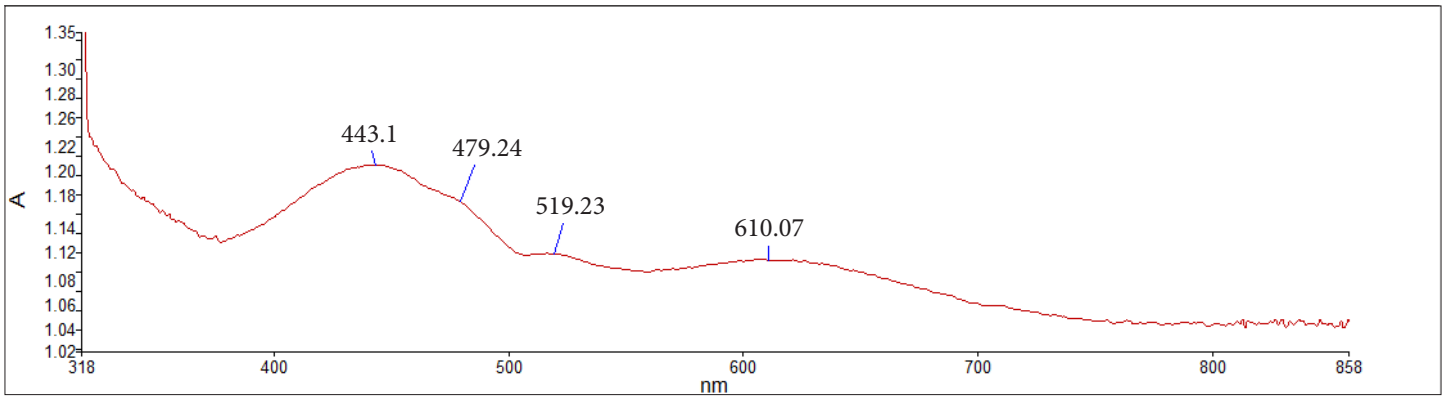

Figure 9a. SRef-060811, green

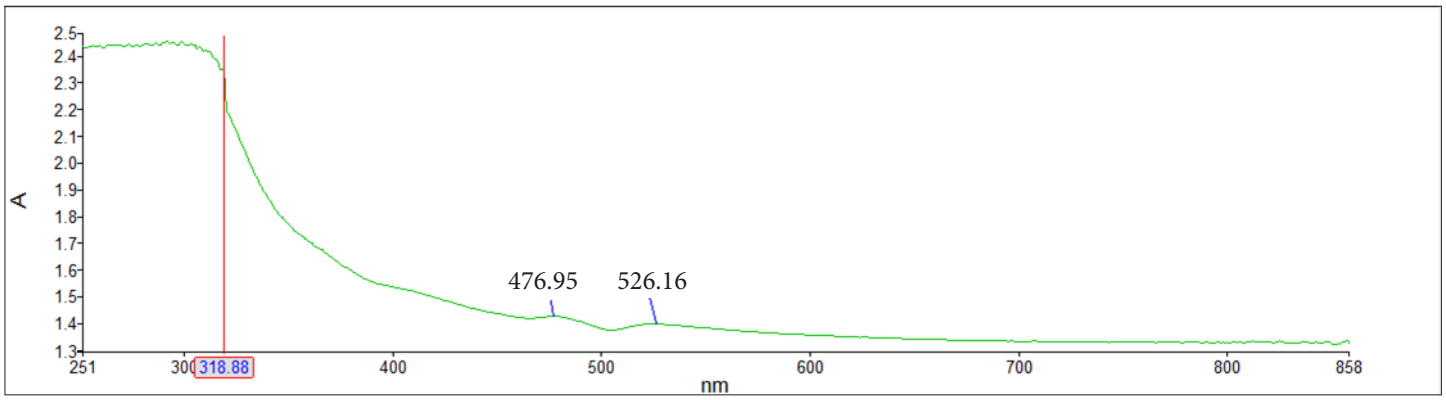

Figure 9b. SRef-060812, bi-color orange and colorless

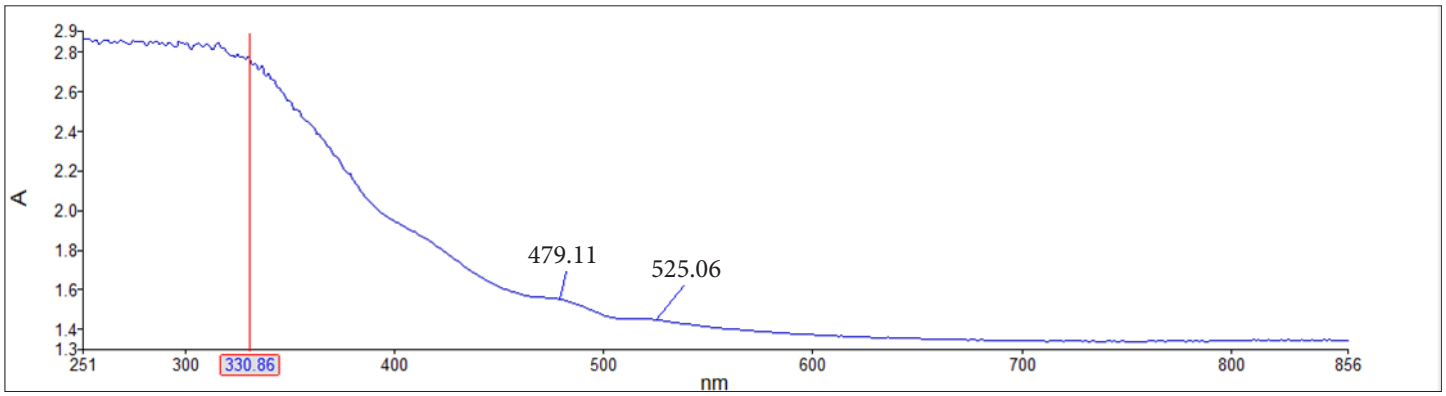

Figure 9c. SRef-060813, bi-color yellow and colorless

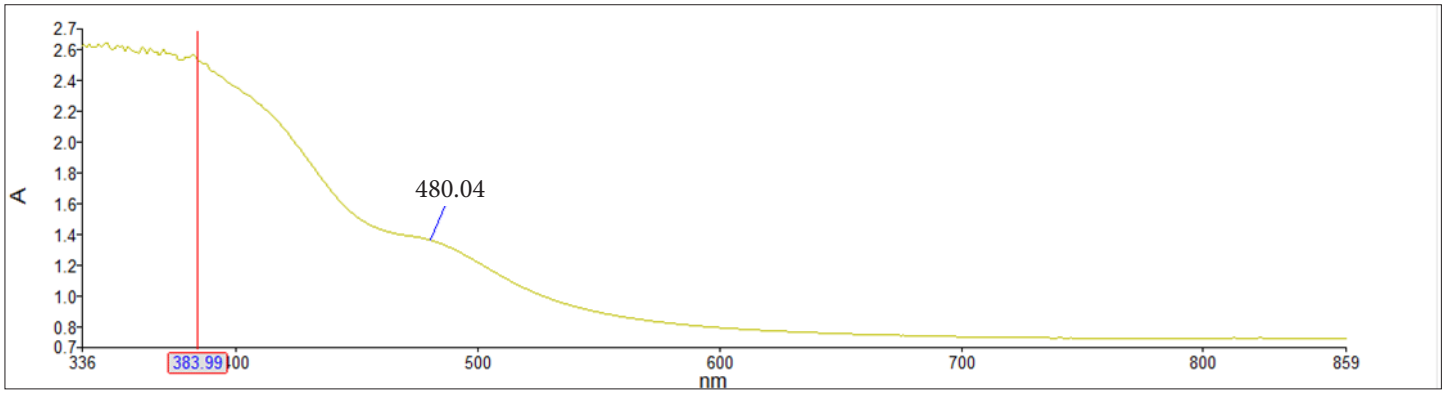

Figure 9d. SRef-060814, orange

DiamondView

Tests using DiamondView were carried out on four samples. All samples react with strong red fluorescence *(Fig.10)* under the short-UV source. Despite the use of different filters, it was impossible to observe any particular crystal growth patterns.

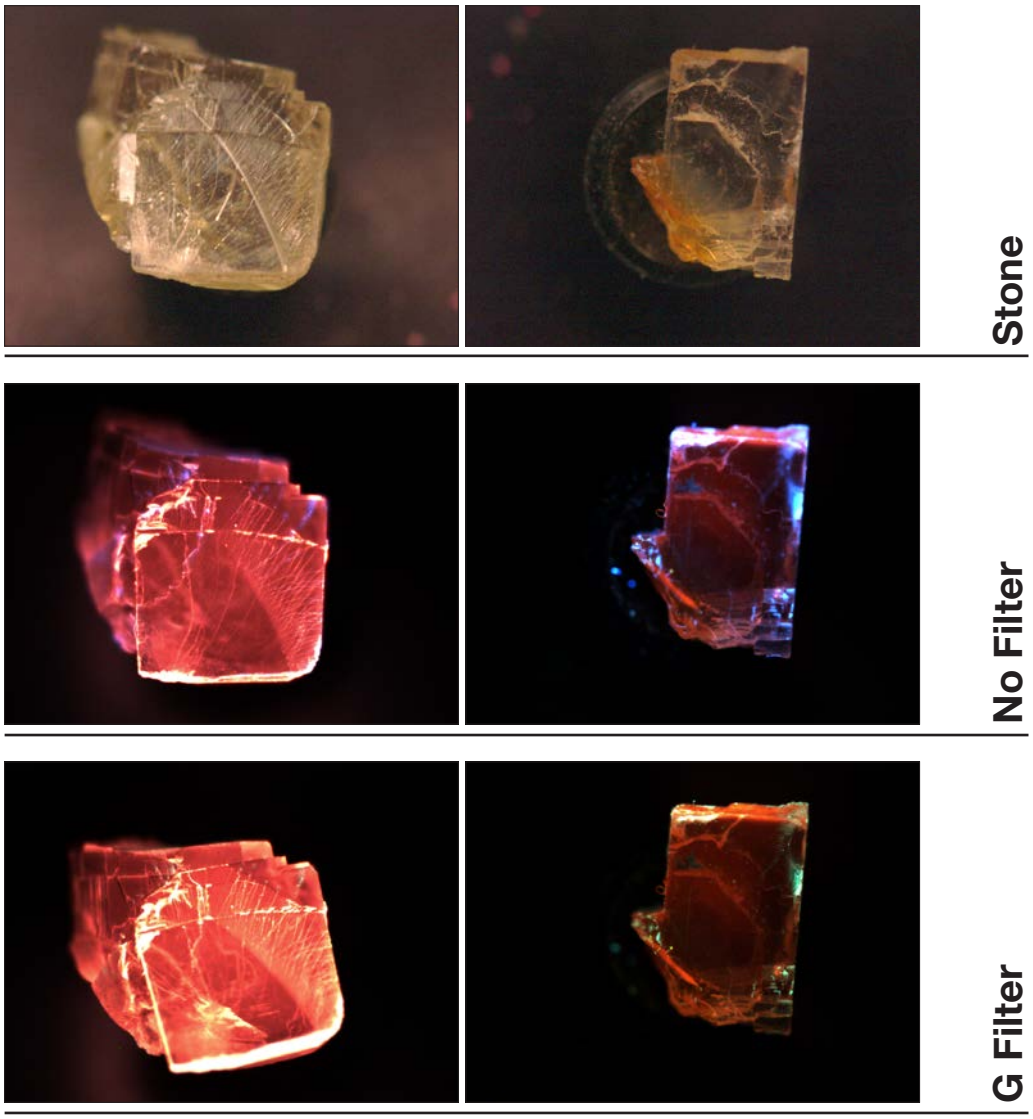

Figure 10. DiamondView image of sample SRef-060812. An uncommonly strong red fluorescent reaction can be observed on all analyzed samples.

Chemical analysis of inclusions in synthetic periclase by SEM-EDS mapping (SRef-060831)

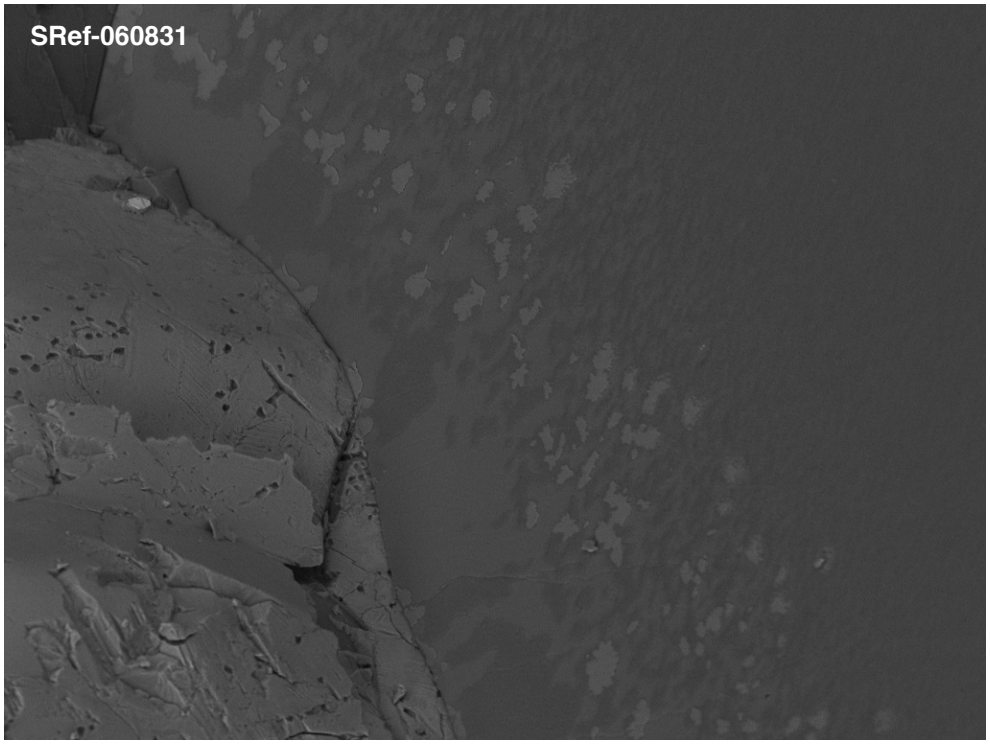

Figure 11. BSE image of a synthetic periclase showing a flame like structure of different solid phases (on the right of the picture) and a solid inclusion on the left side. The small flames are about 10 µm and the inclusion on the left was well visible under light microscopy. To expose it for SEM, we broke the synthetic periclase into two pieces. The SEM-EDS mapping showed a regular pattern of flames consisting of **Mg** *(a)*, **Ca** *(b)* and **O** *(d)* representing **Ca-Mg-Carbonate**. **C** is not shown in the mapping because the sample was coated with carbon *(see Materials & Methods)*.

A second type of inclusion consists of **Fe-Ni-P** particles *(f, g and h)* and the third larger inclusion is a **Ca-Si-Oxide** *(b and c)*.

Mg K Series

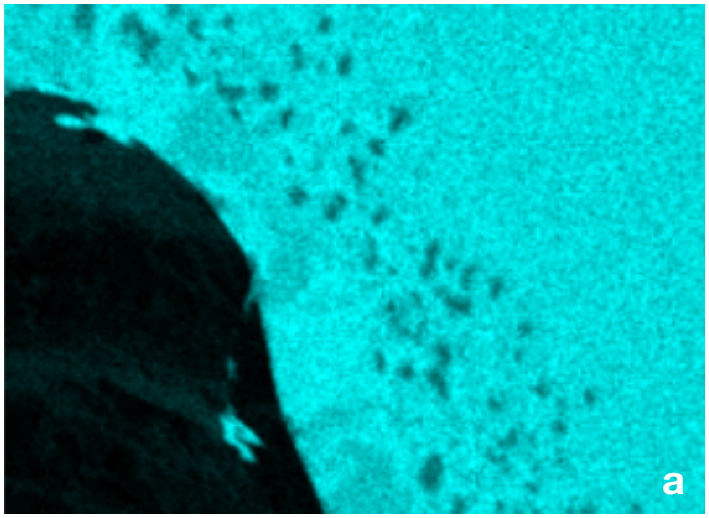

Ca K Series

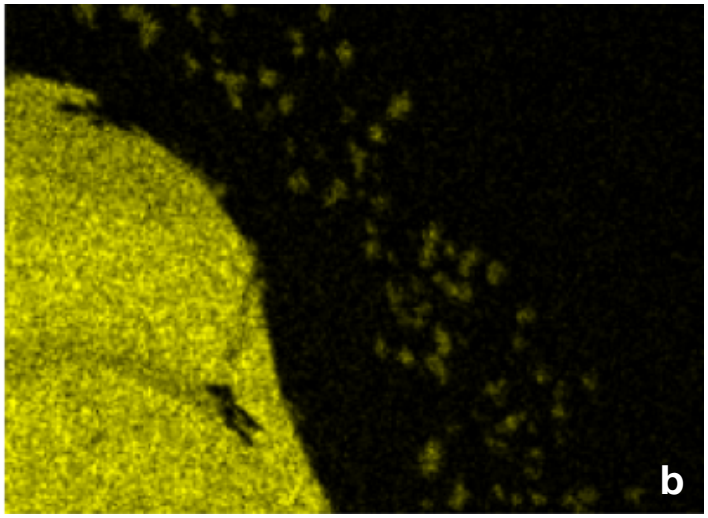

Si K Series

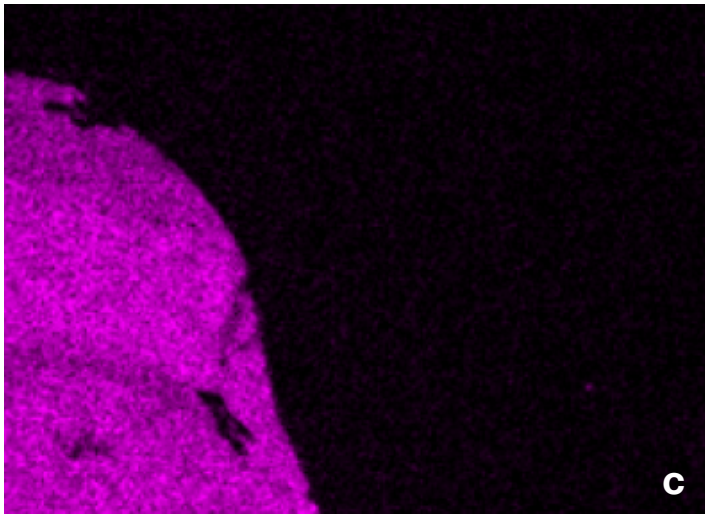

O K Series

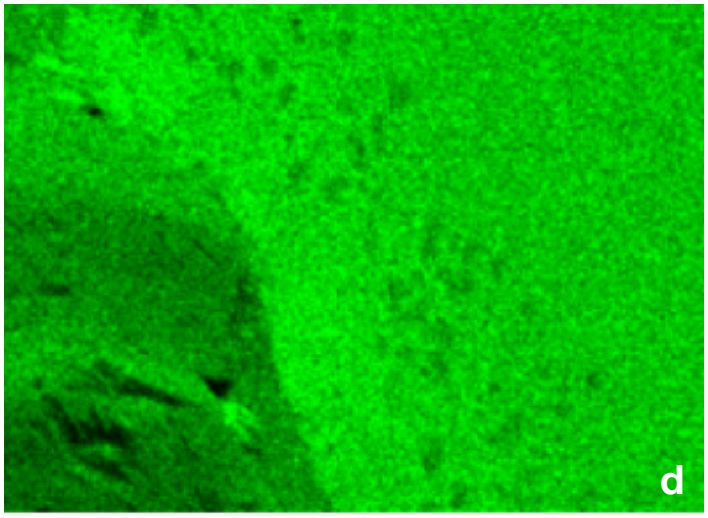

F K Series

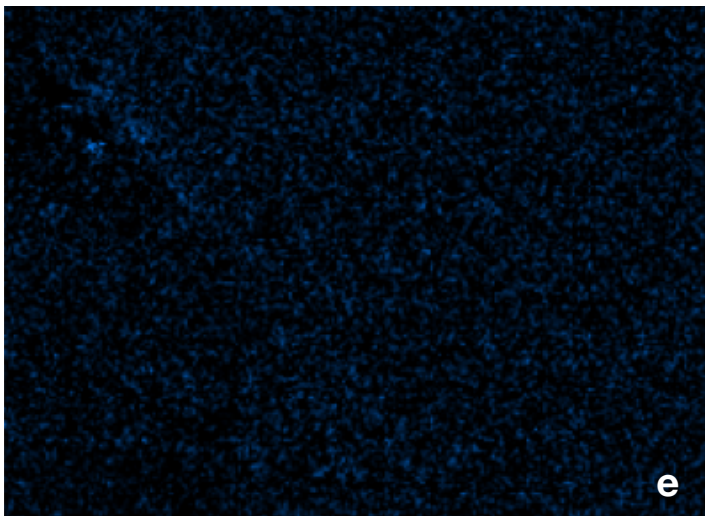

P K Series

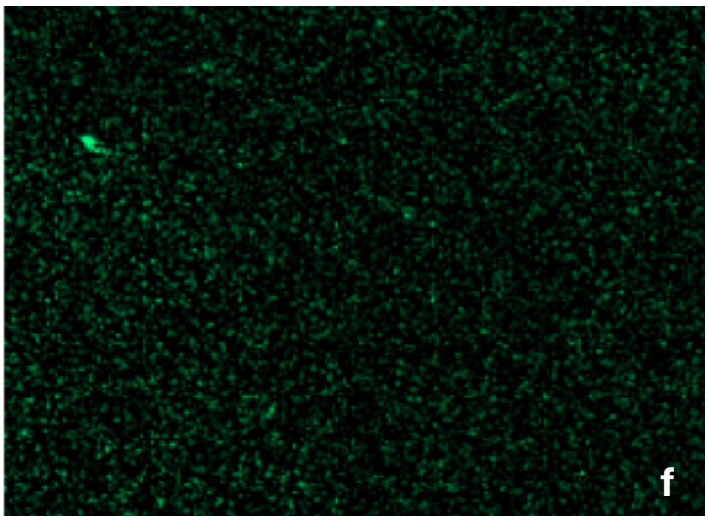

Fe L Series

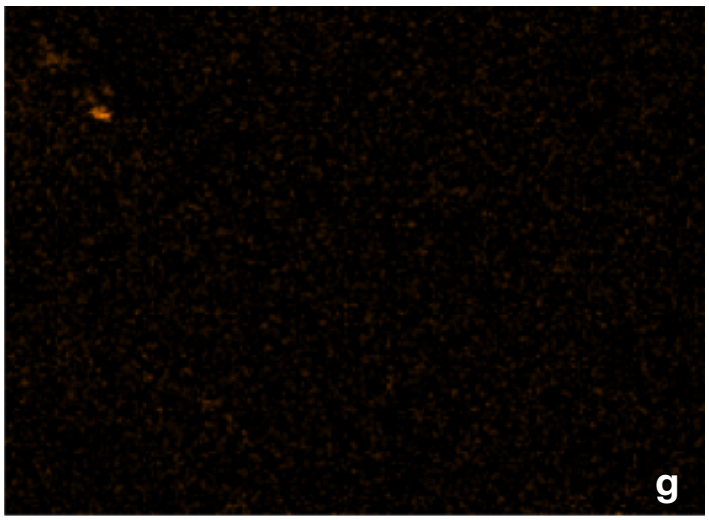

Ni L Series

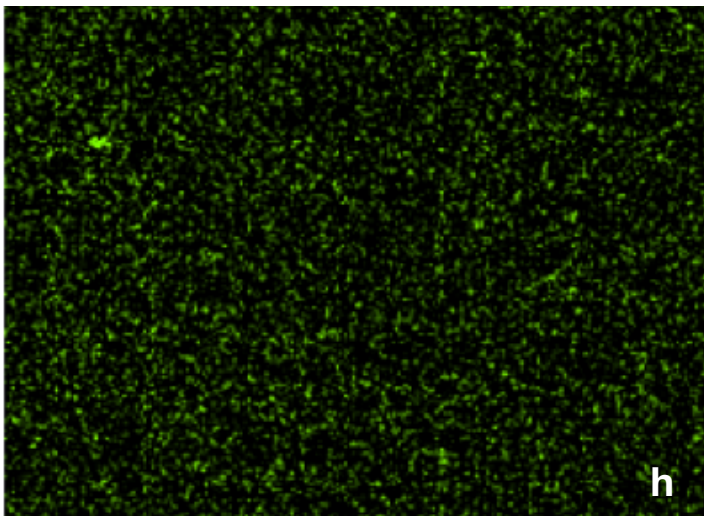

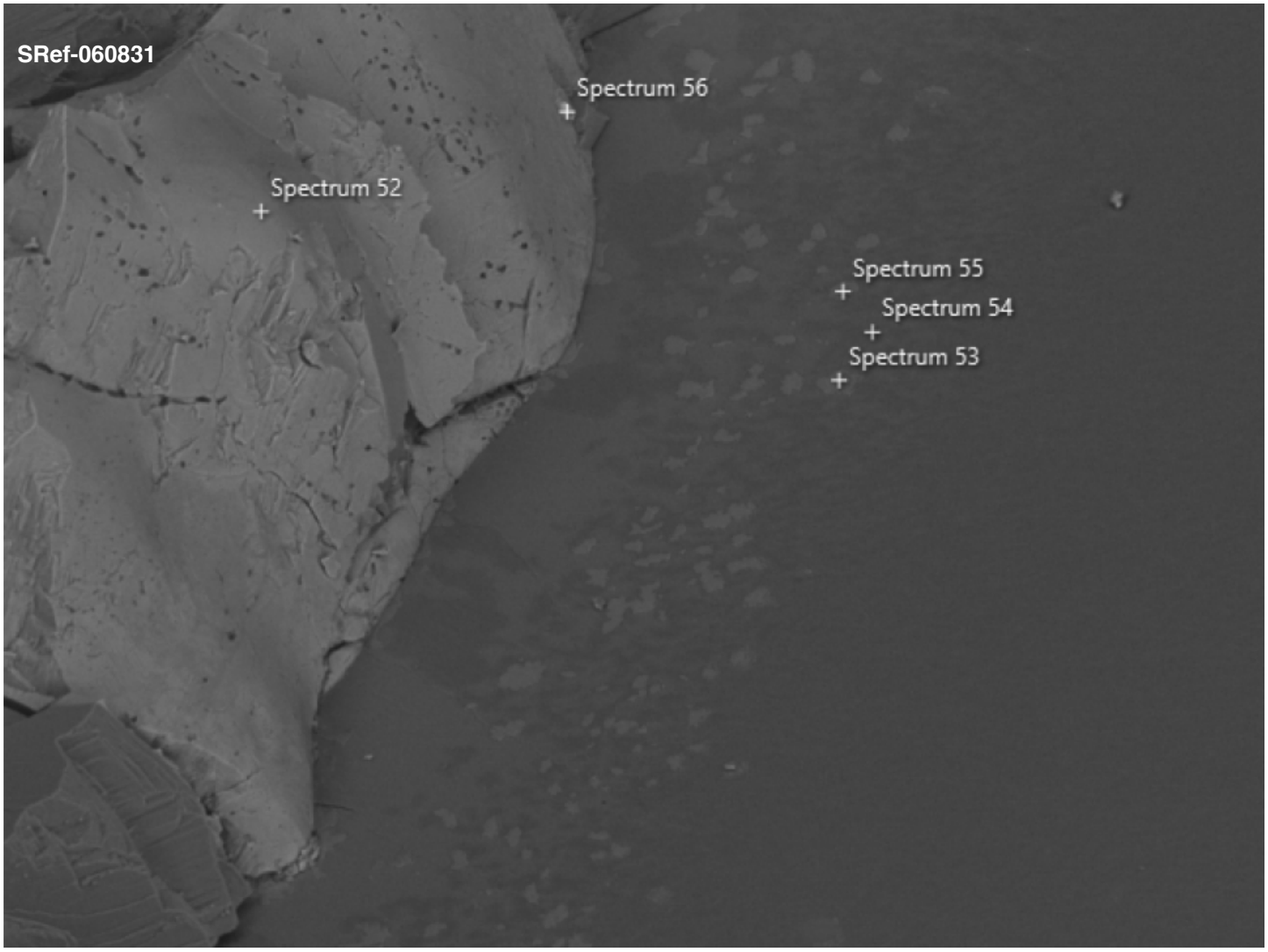

Figure 12a. Same area as seen in Fig. 11. but with the location of SEM-EDS point measurements. The SEM-EDS spectra show the presence of a Ca-Si-particles as well as areas with Ca-Mg, Ca-Mg-Fe-Ni-P compositions in flame like or exsolved features within the synthetic periclase (inserted above the image of the sample tested). Elements detected on point 52 (Ca, Si, O), point 53 (Ca, Mg, O), point 54 (Mg, O), point 55 (Mg, Ca, O), point 56 (Fe, Ni, Ca, P, Si Mg, F, O). Note the presence of Fe- and Ni-concentrations in point 56.

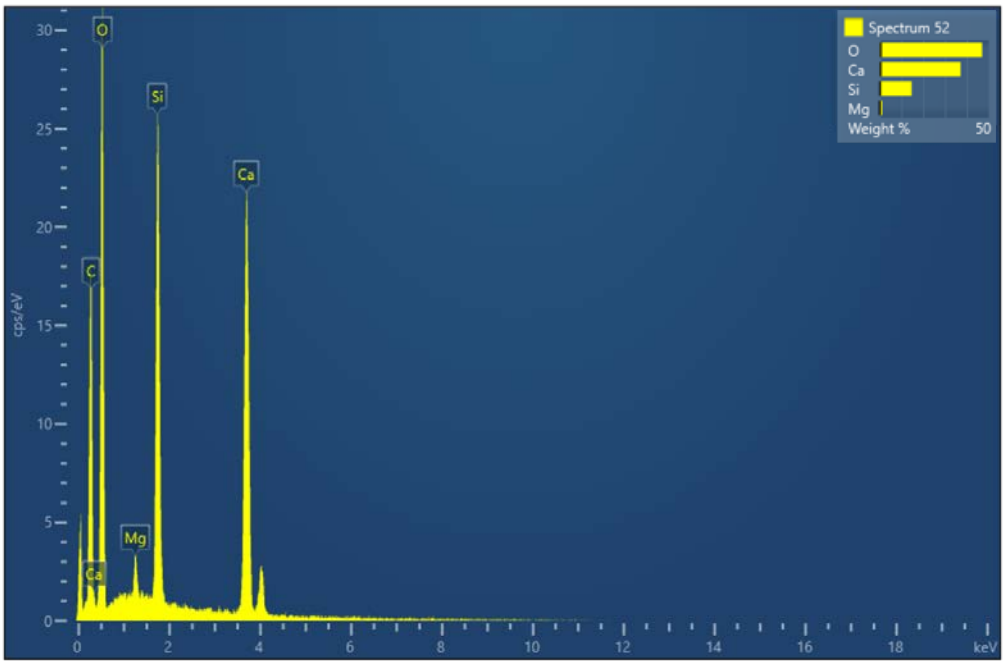

Figure 12b. SEM-EDS analysis of inclusion at point 52 (see Fig. 12a) including quantitative analysis.

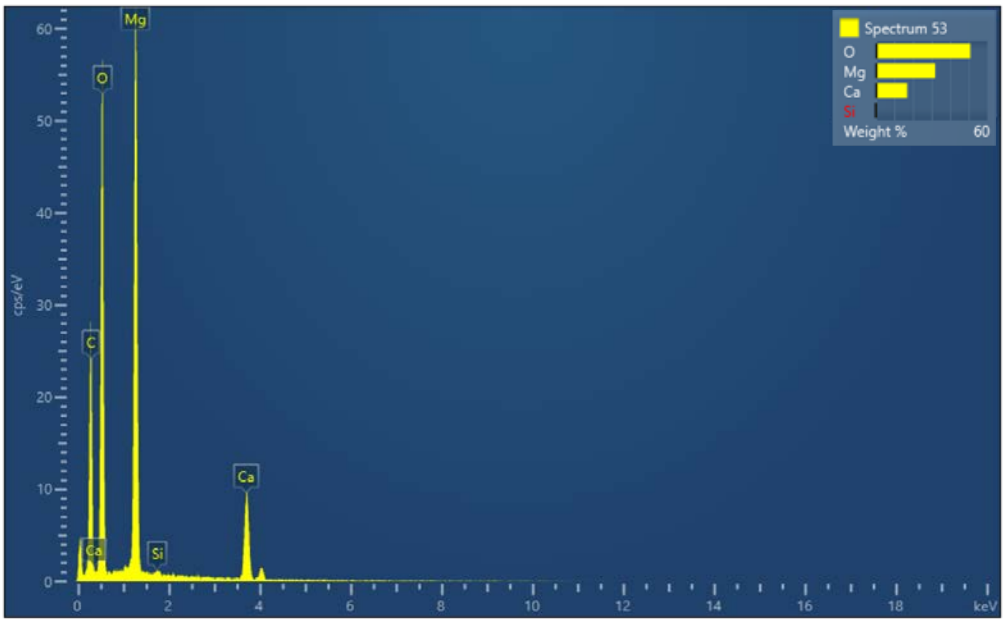

Figure 12c SEM-EDS analysis of inclusion at point 53 (see Fig. 12a) including quantitative analysis.

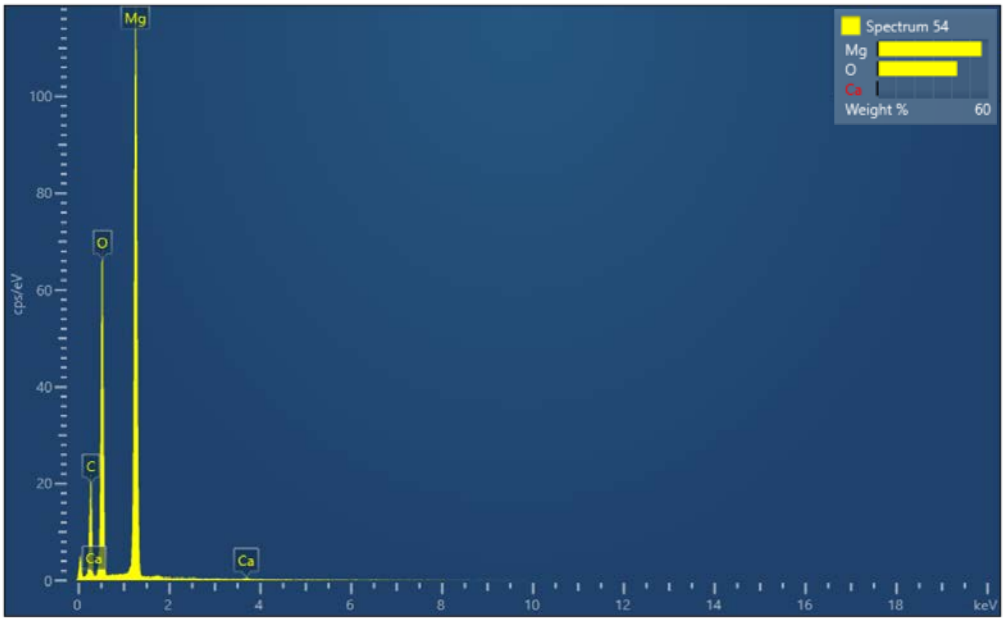

Figure 12d. SEM-EDS analysis of inclusion at point 54 (see Fig. 12a) including quantitative analysis.

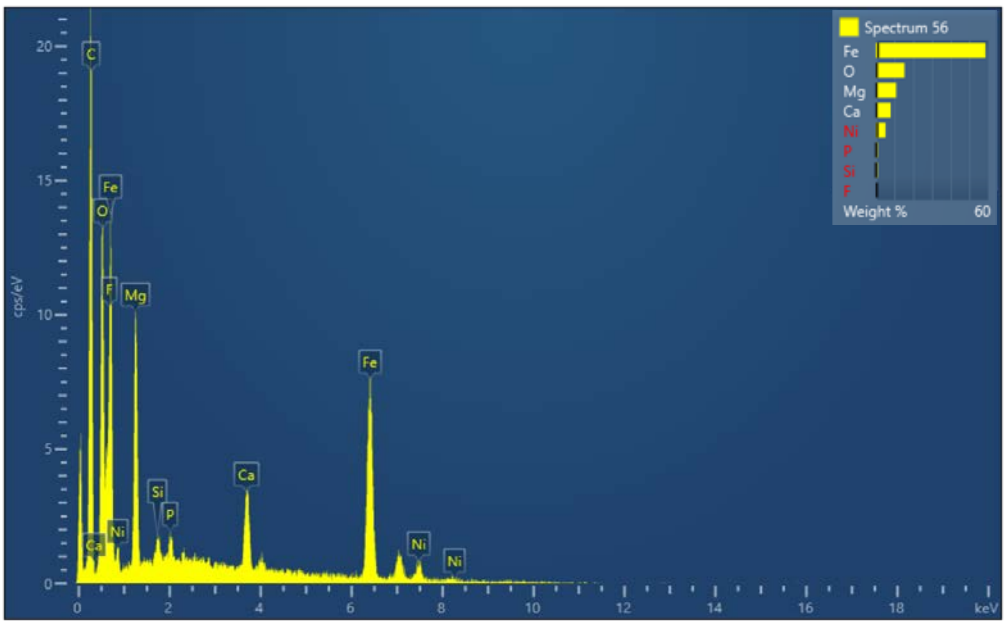

Figure 12e. SEM-EDS analysis of inclusion at point 56 (see Fig. 12a) including quantitative analysis.

Figure 13a. Overview of point measurements by SEM-EDS surrounding an inclusion in synthetic periclase. Raman and SEM were acquired on the same inclusion (labeled as spectrum 50).

Detection of the following elements on point 45 (element O, Fe, Mg), point 46 (O, Fe, Mg, P), point 47 (O, Fe, Mg), point 48 (Mg, O), point 49 (Fe, P, Mg, Ni, O), point 50 (Ca, Si, O), point 51 (Mg, O).

Note: The chemical composition of point 49 are complex Ni- and Fe-bearing phosphates that are interpreted as synthetic and need further analysis. Possibly it is a phosphorous bearing rubber particle that contaminated the synthetic particle during the production process *(Drück et al., 2017)*.

The "rubber" is overgrown by needles of pure magnesium oxide (periclase) at point 48.

The elemental concentration of carbon (C) has not been investigated due to carbon coating of the samples.

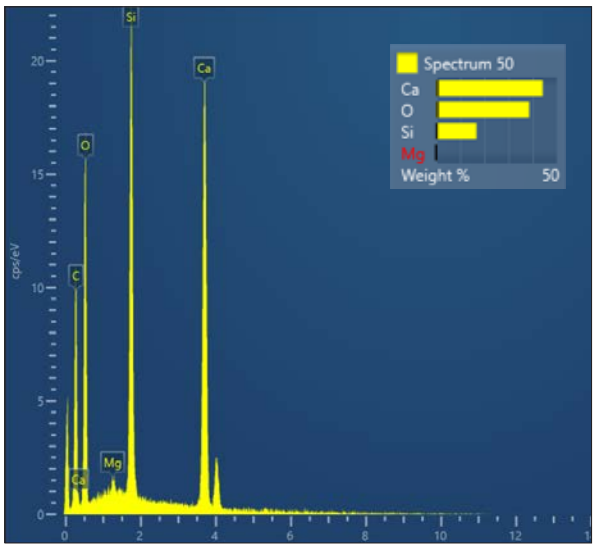

Figure 13b. SEM-EDS analysis of inclusion at point 50 *(see Fig. 13a)* including quantitative analysis.

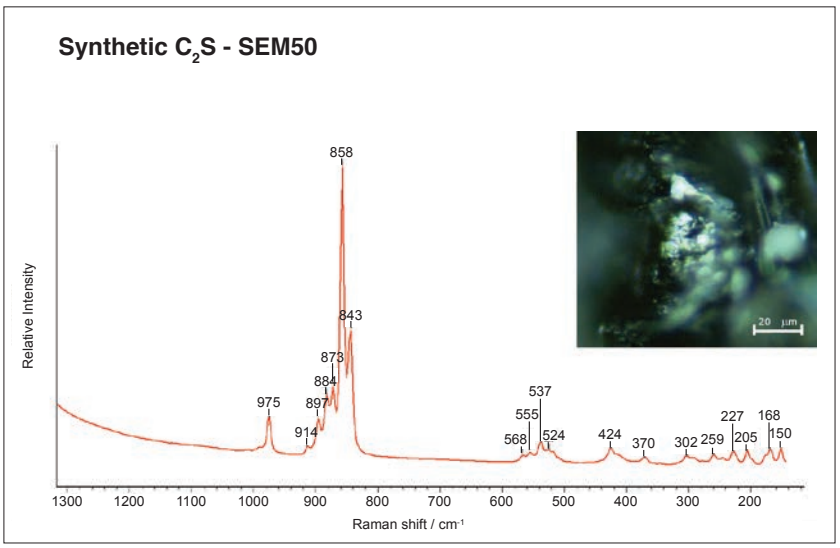

Figure 13c. Raman spectrum of inclusion point No. 50 (see Fig. 13a) identified as C_2S dicalcium silicate (cement hardener).

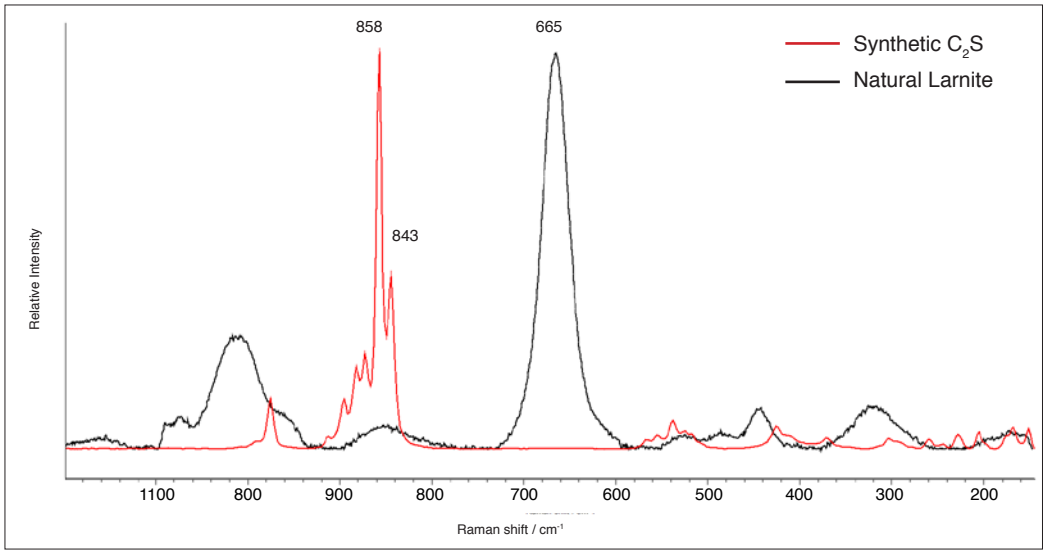

Figure 13d. Overlay of two different Raman spectra of the polymorph's of dicalcium silicate (synthetic C_2S and natural larnite). In red is the reported C_2S spectrum acquired from the same particle as reported in Fig. 13c. The black spectrum is a re-plot of the larnite mineral phase, published by Michael Scott on RRUFF spectra database *(R070530)*. The main doublet bands in the C_2S spectra are at 858 and 843 cm^{-1} and are completely different from the larnite spectrum which shows the main band at 665 cm^{-1}. Raman spectroscopy offers conclusive results for distinction of synthetic C_2S and natural larnite.

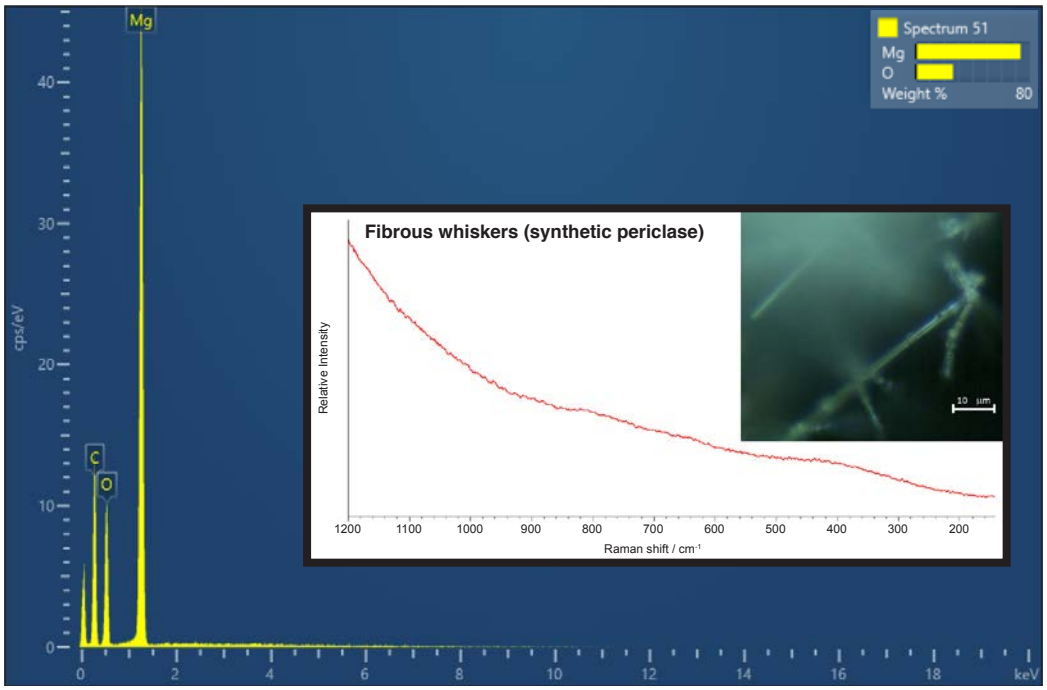

Figure 13e. (inlay) Raman spectrum obtained by focusing the laser source on the fibrous inclusions, analyzed before by SEM-EDS and reported in optical microscopy image in the box. Despite of the well-formed prismatic habit of the crystals, no Raman bands are clearly visible.

Note: The SEM-EDS spectra measured on different positions of a complex inclusion revealed different phosphates, Fe-Mg solid materials, fibrous whiskers of periclase and Ca-Si-bearing solid materials (spectrum 50).

The latter was identified as C_2S by Raman spectroscopy. Only the polymorph "larnite" occurs in nature, in contact-metamorphism of limestones. Due to the Raman spectra acquired larnite can be excluded. All other polymorph's of C_2S solid crystals are not known in nature but well-known in the cement industry *(see discussion)*.

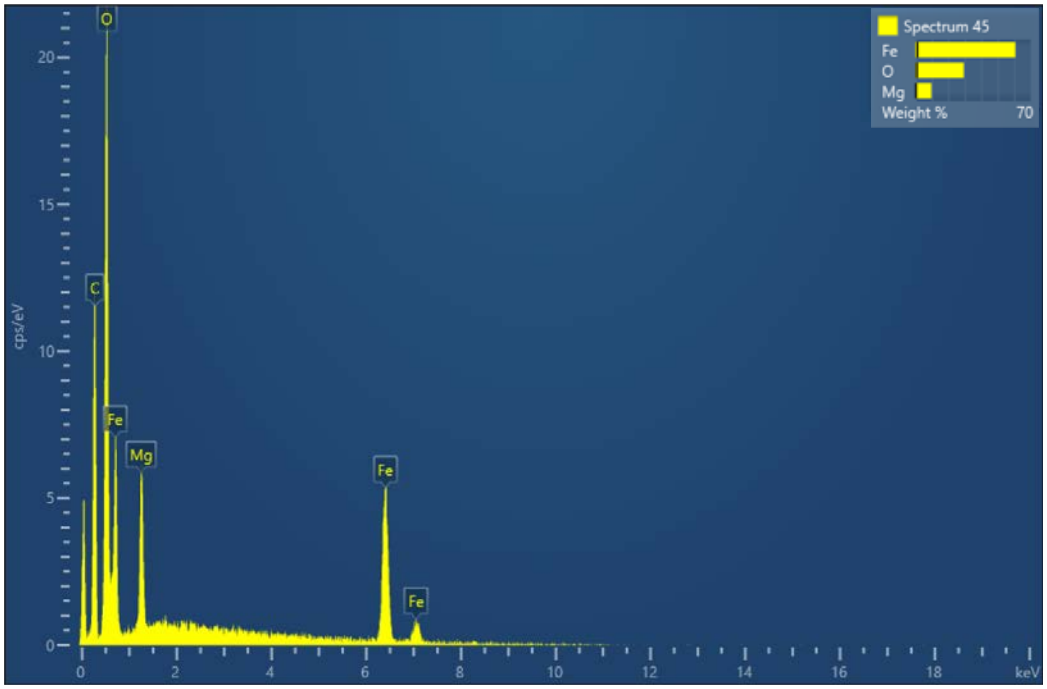

Figure 13f. SEM-EDS analysis of inclusion at point 45 *(see Fig. 13a)* including quantitative analysis.

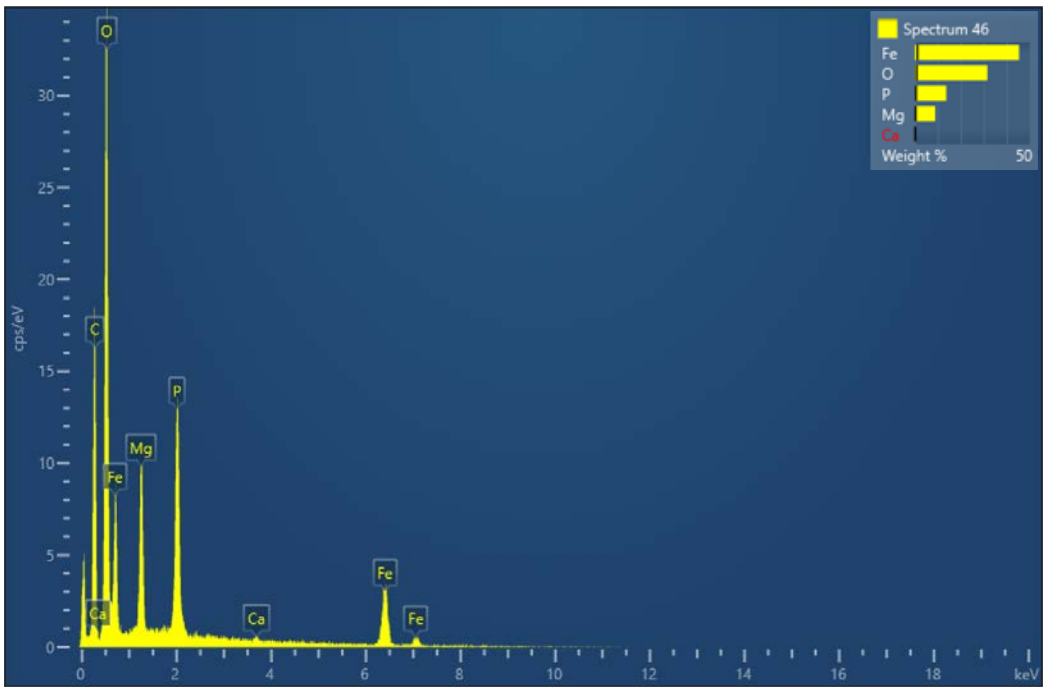

Figure 13g. SEM-EDS analysis of inclusion at point 46 *(see Fig. 13a)* including quantitative analysis.

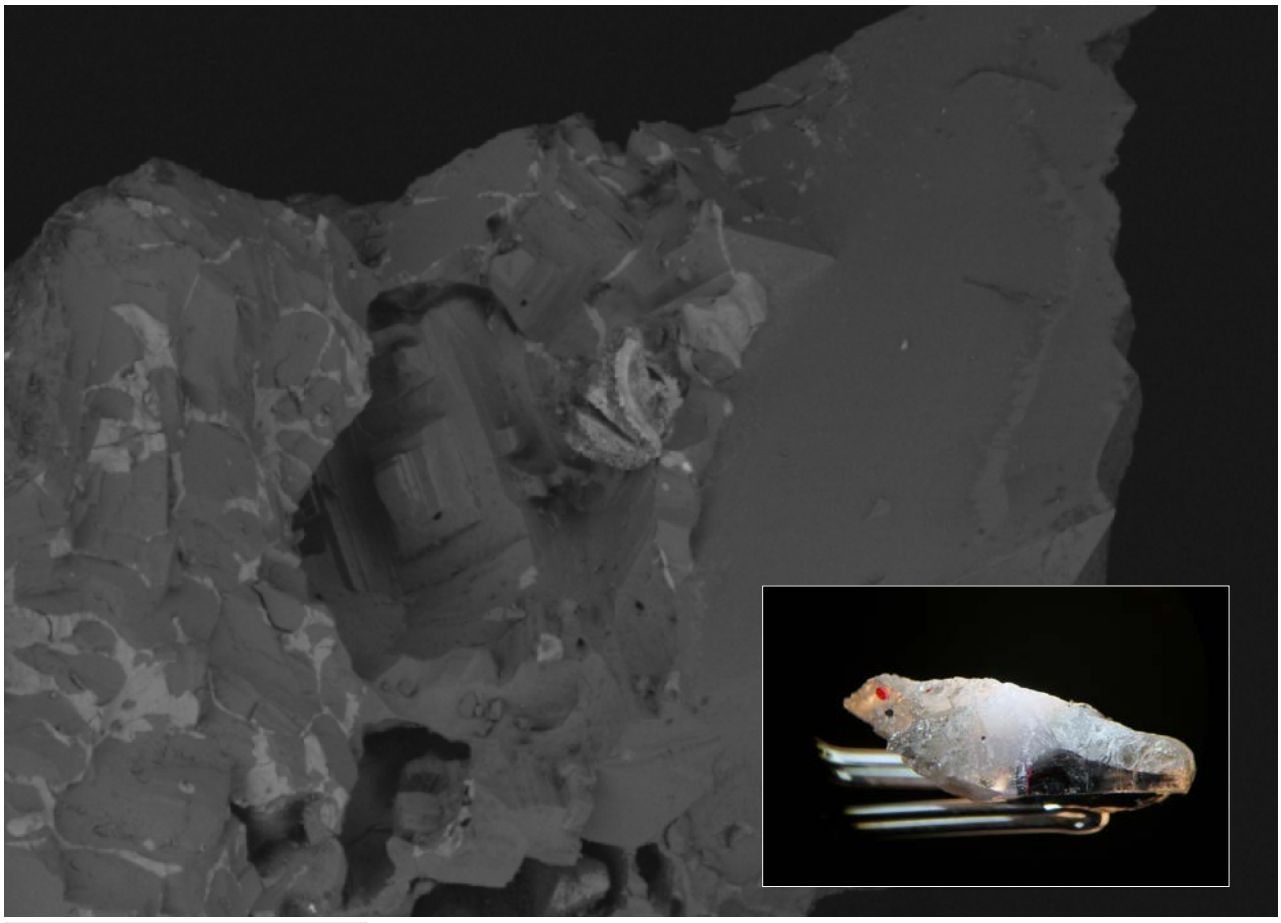

Figure 14a. SEM-Image of synthetic periclase showing different gray tones due to chemical differences. Other position produced by rotating the sample *(Fig. 14b)*. **(Inlay)** macro image of the analyzed synthetic periclase.

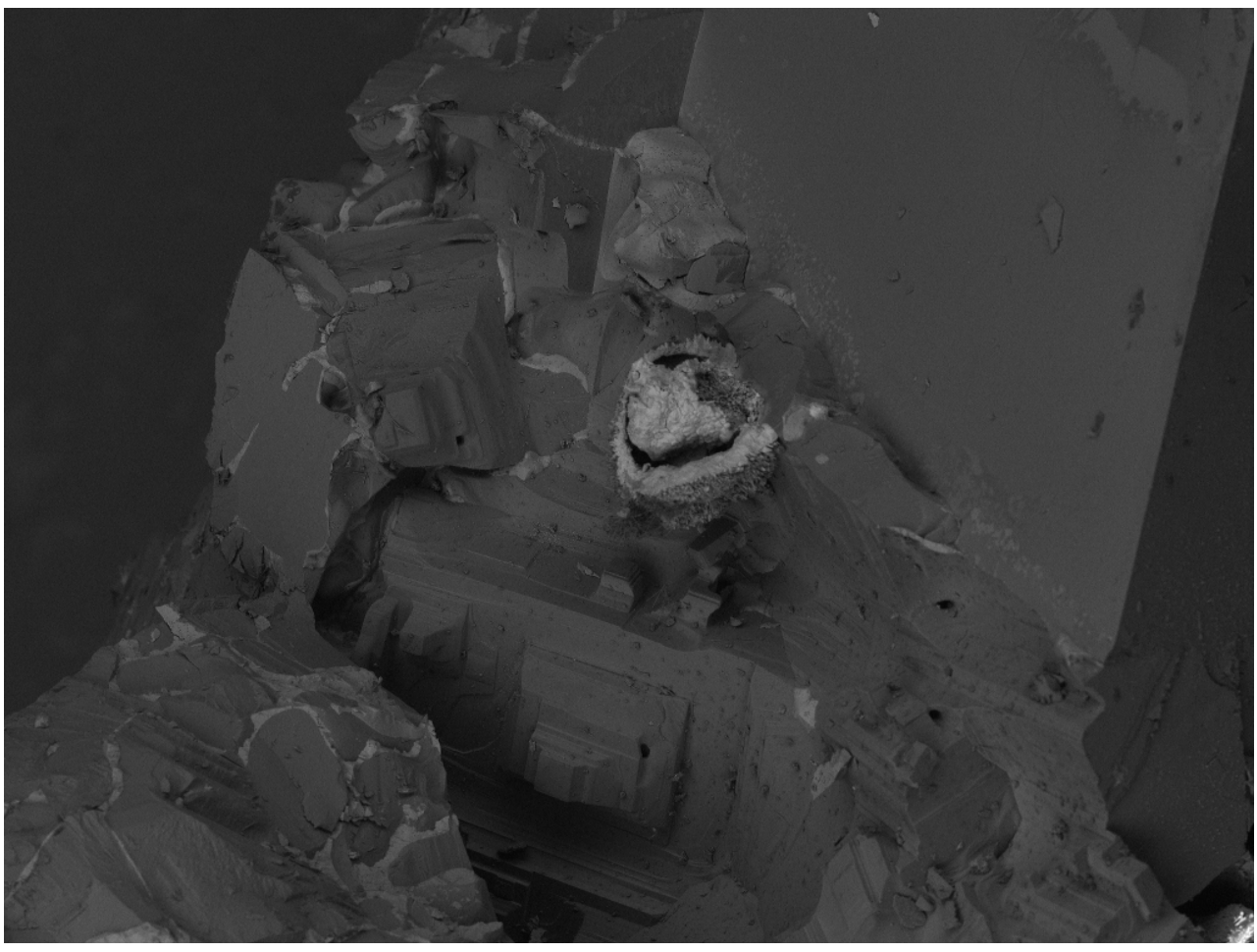

Figure 14b.

Figure 14c. SEM-BSE image of a synthetic periclase showing a network of veins and a solid inclusion in the centre of approx. 0.5 mm. To expose the inclusion we broke the synthetic periclase into two pieces. The SEM-EDS mapping showed the veins consisting of **Ca** *(picture e)* **Si** *(f)*, and **O** *(g)* representing **Ca-Si-oxide** solid materials. The centrally located inclusion consists of **Fe-P** and **Ni-particles** *(picture i, j and k)*.

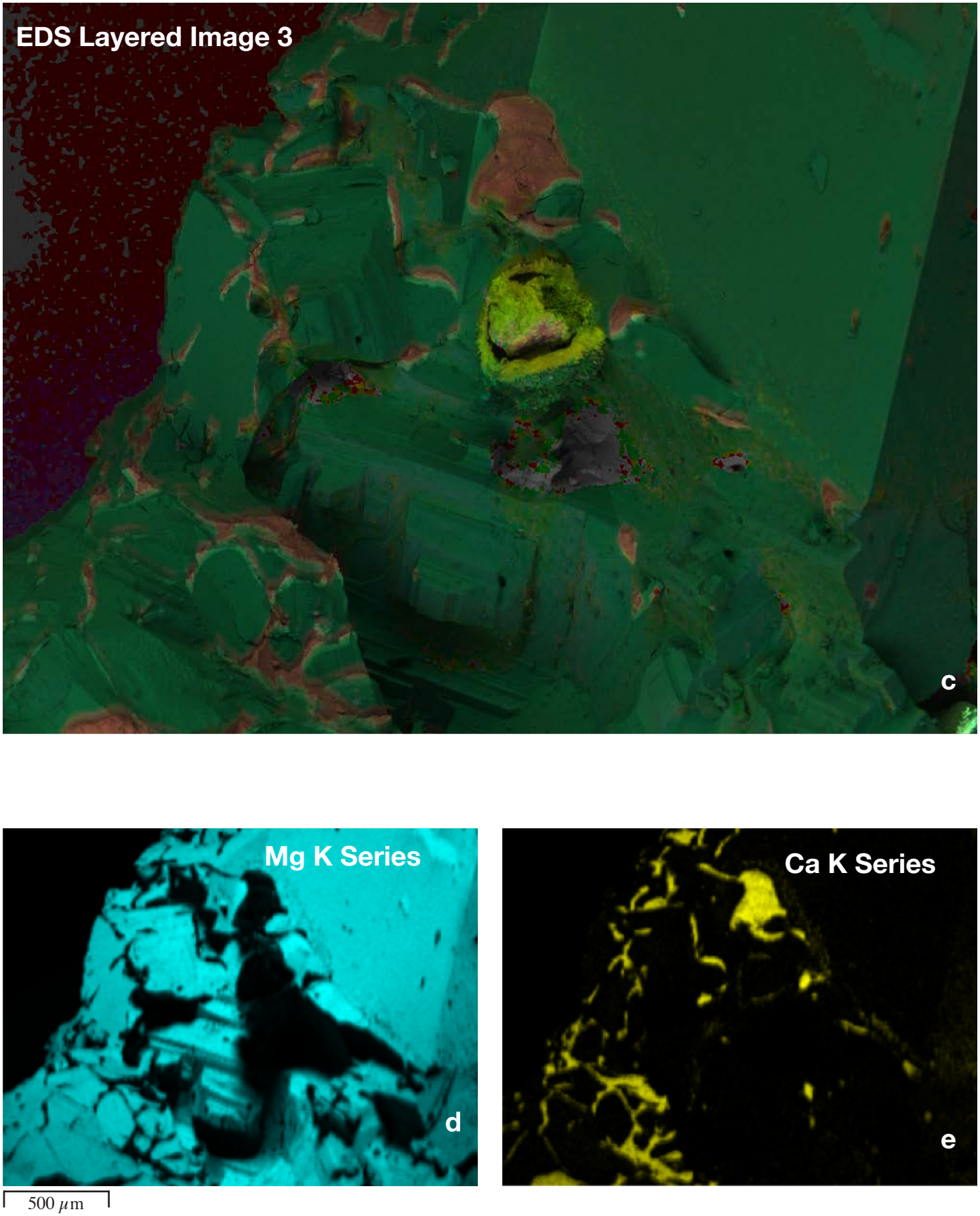

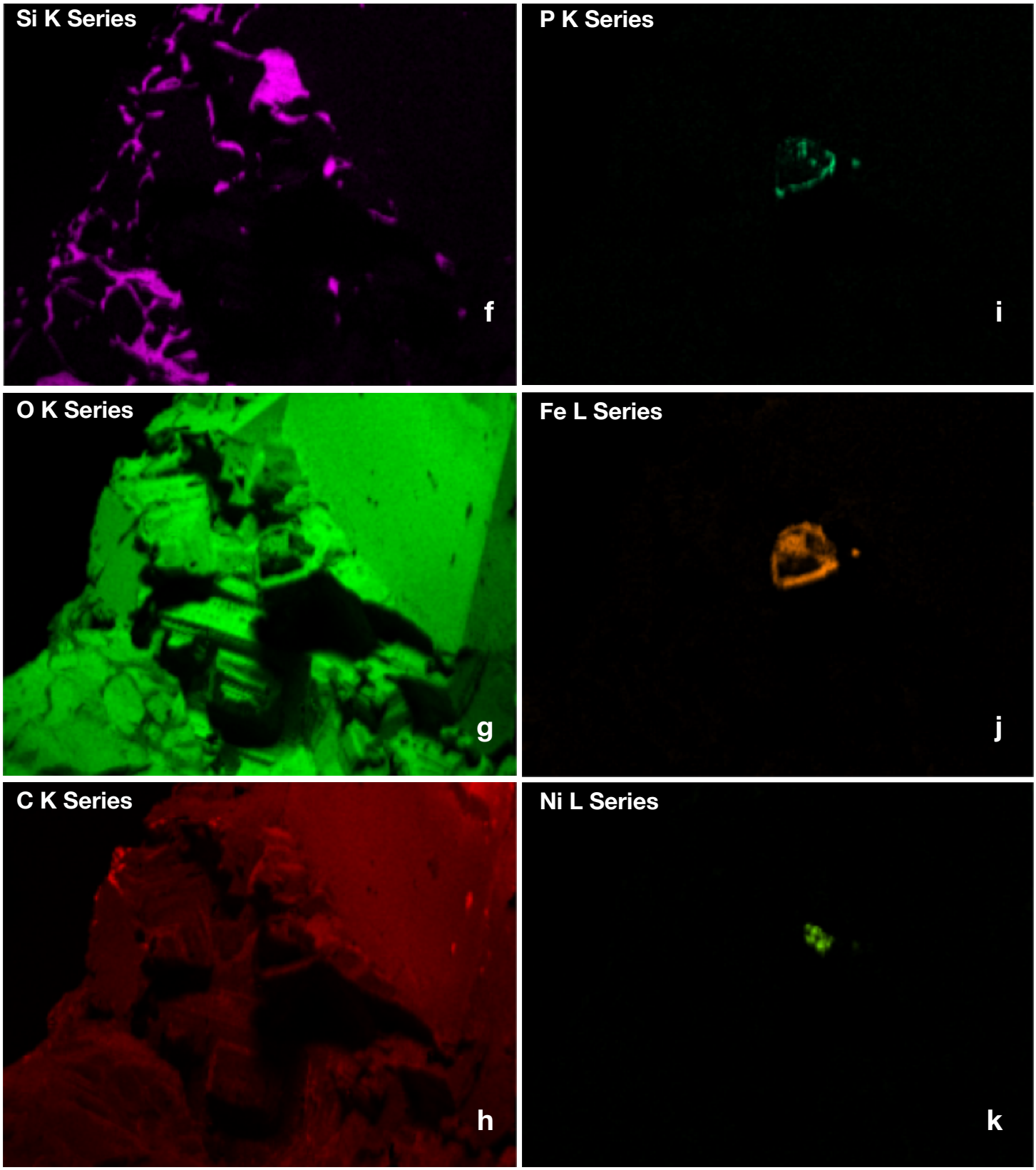
Si K Series
f
P K Series
i
O K Series
g
Fe L Series
j
C K Series
h
Ni L Series
k
500 μm

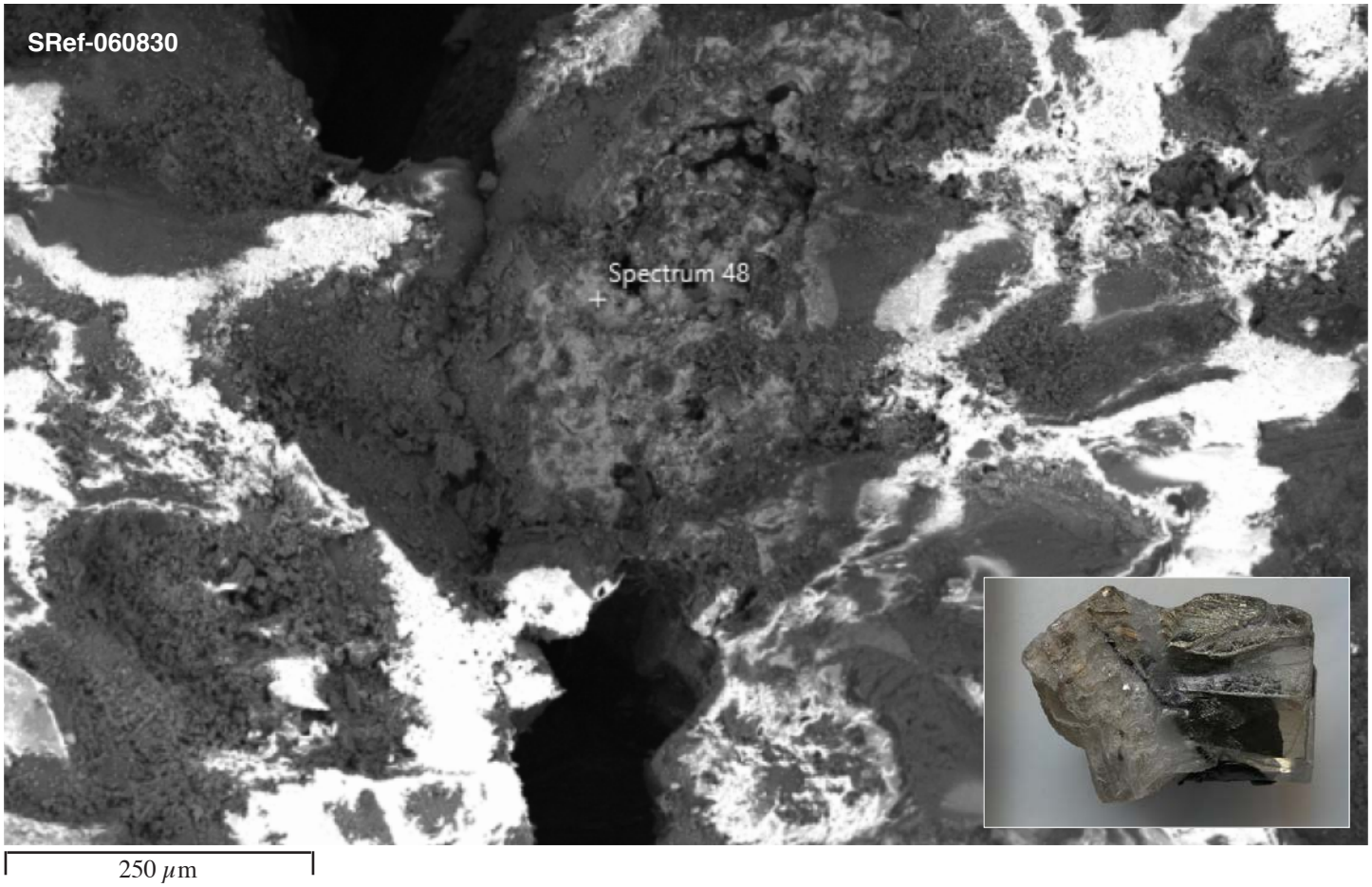

Figure 15. SEM-SE picture of black inclusion in synthetic periclase was identified as hematite by combined SEM-EDS and Raman spectroscopy. SRef-060830.

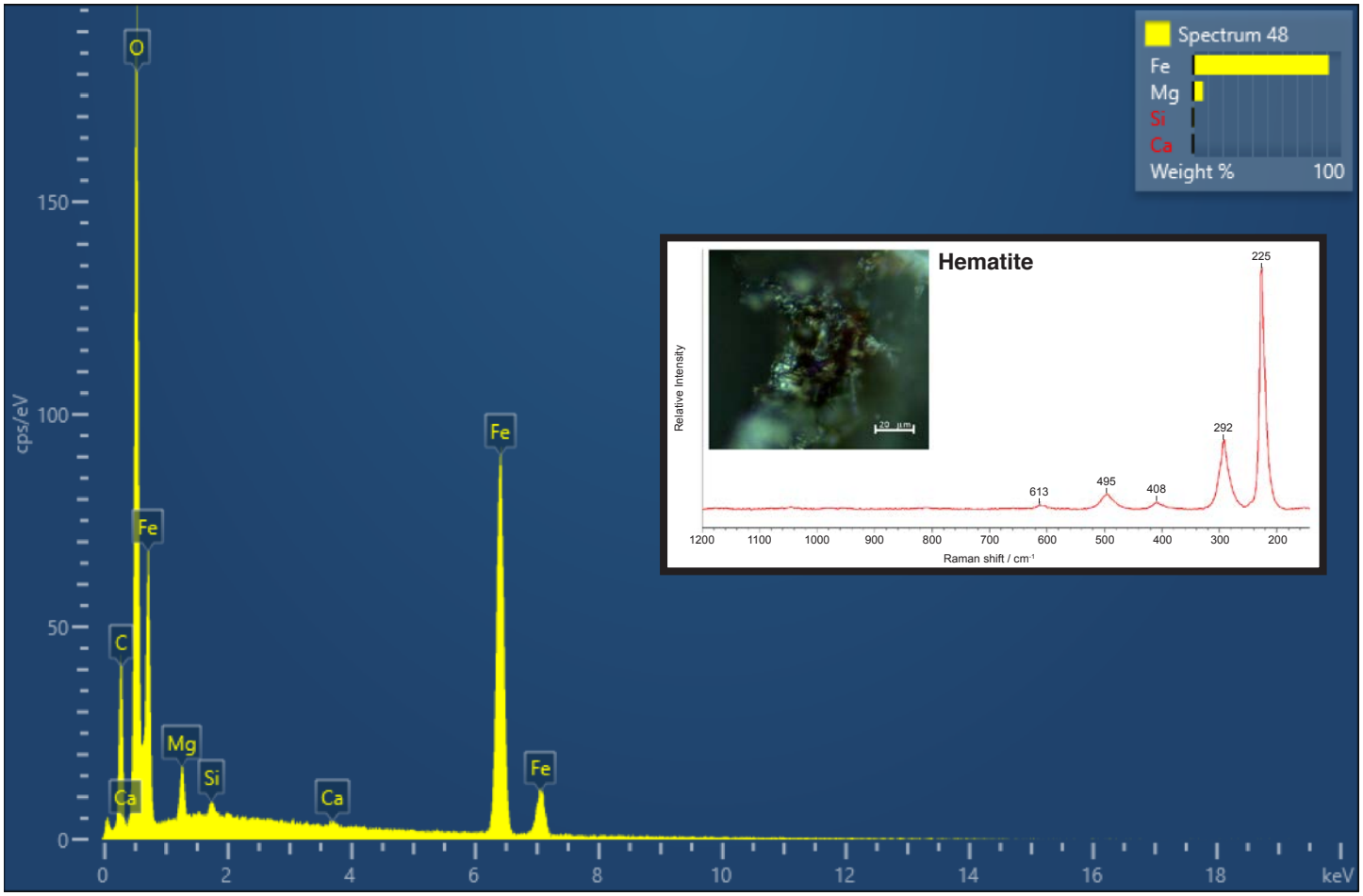

Figure 16. SEM-EDS signal and semi-quantitative analysis of inclusion 48 (see Fig. 15). Inserted is the Raman spectrum of the same inclusion. On the basis of the references *(Shubnel, 1992)*, the main bands at 225, 292, 408, 495 and the broad band at 613 cm^{-1}, it was identified as hematite.

Figure 17a.

Figure 17b. Macro image of the analyzed synthetic periclase. Red circle details the position of the analyzed inclusion.

Figure 17a. SEM-SE image of a porous part of a synthetic periclase. The material in the veins surrounding this void contain Ca-Si *(Fig. 18b)*. Raman spectroscopy identified the substance as C_2S *(Fig. 18a.)*, a well-known material in the cement industry. This element does not occur in nature and prove s the synthetic origin of this periclase.

Detection of the following elements on point 57 (Ca, Si, Mg, O) and point 58 (Ca, Si, minor Mg).

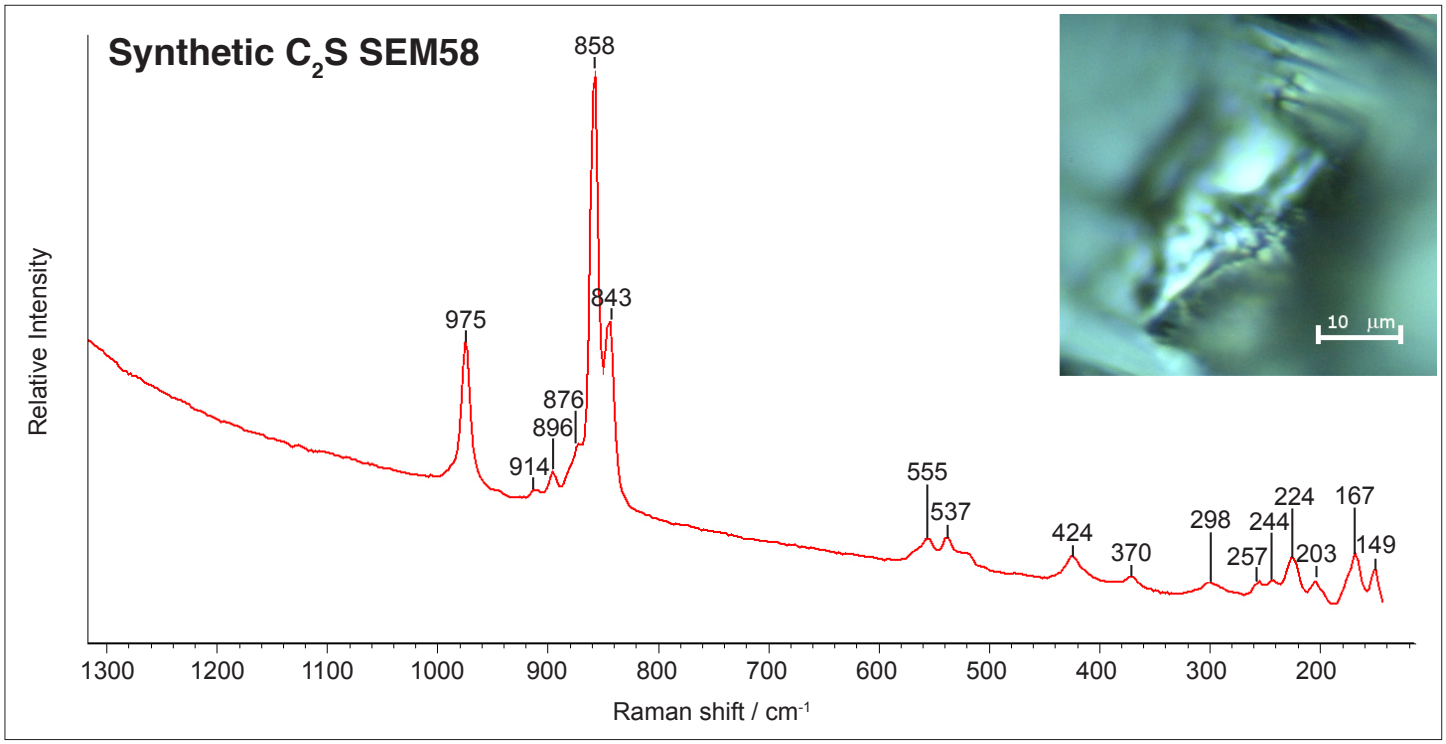

Figure18a. Raman spectrum of point 58 *(see Fig. 17a)* revealed bands ascribable to Portland cement products, called C_2S (dicalcium silicate).

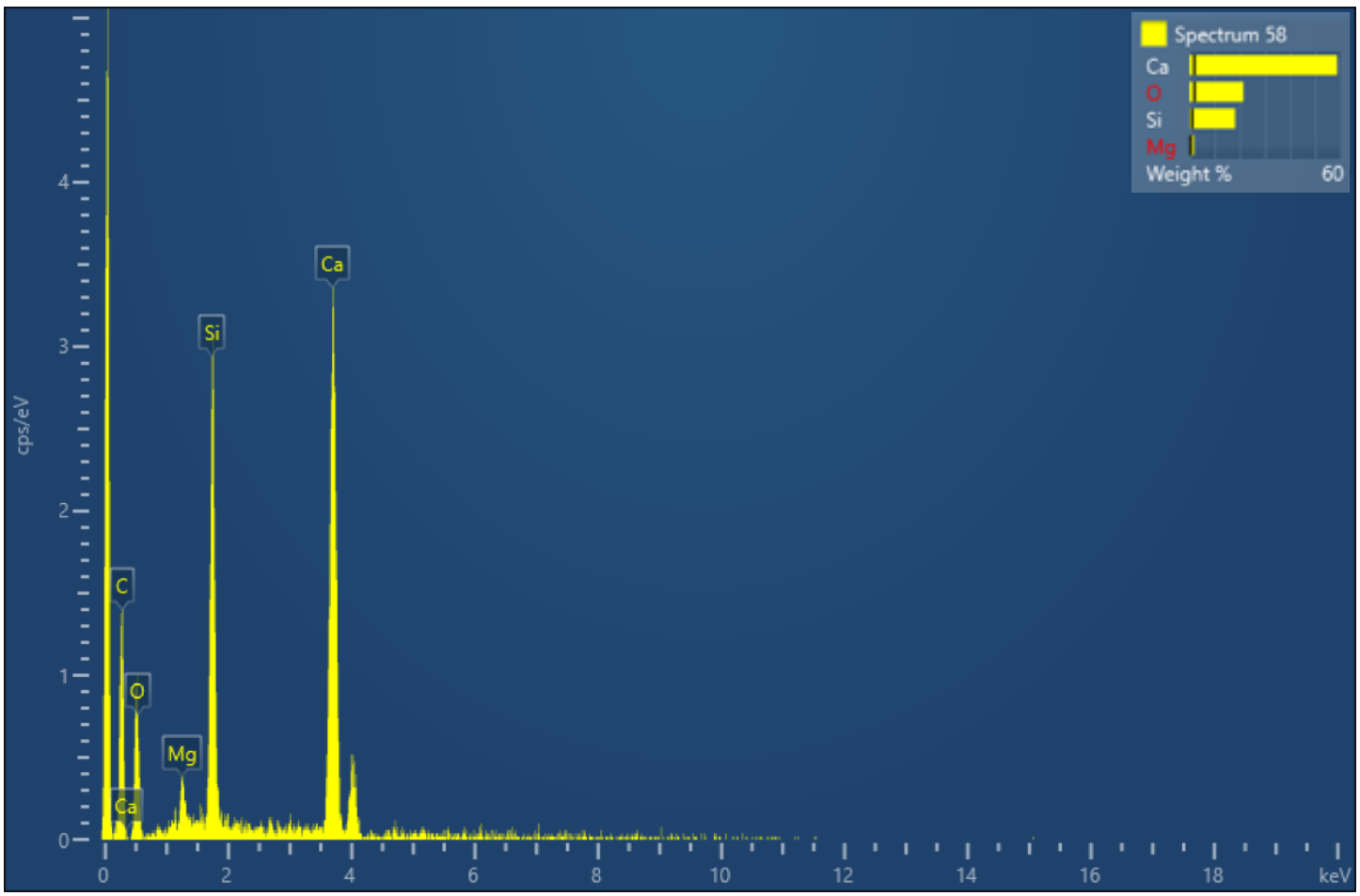

Figure 18b. SEM-EDS analysis of inclusion at point 58 *(see Fig. 17a)* including quantitative analysis.

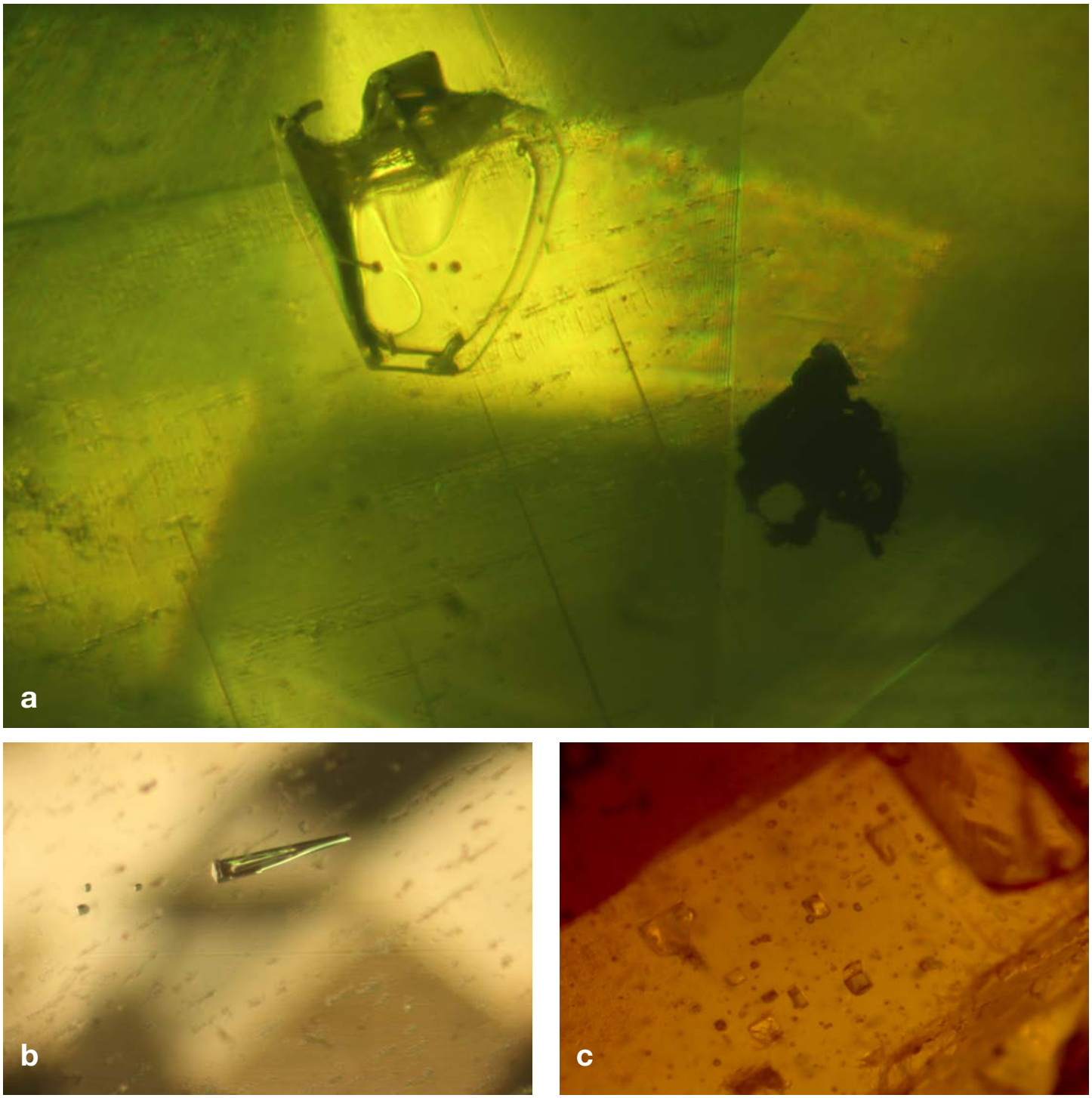

Figures 19a-c. Micro-photograph of fluid inclusions in different colored synthetic periclase. Multi-phase fluid inclusions with different unmixed liquids and gas phases at room temperature **(a)**. Triangular shape fluid inclusions **(b)** and rectangular fluid inclusions **(c)**. First identification attempts see Figures 20.

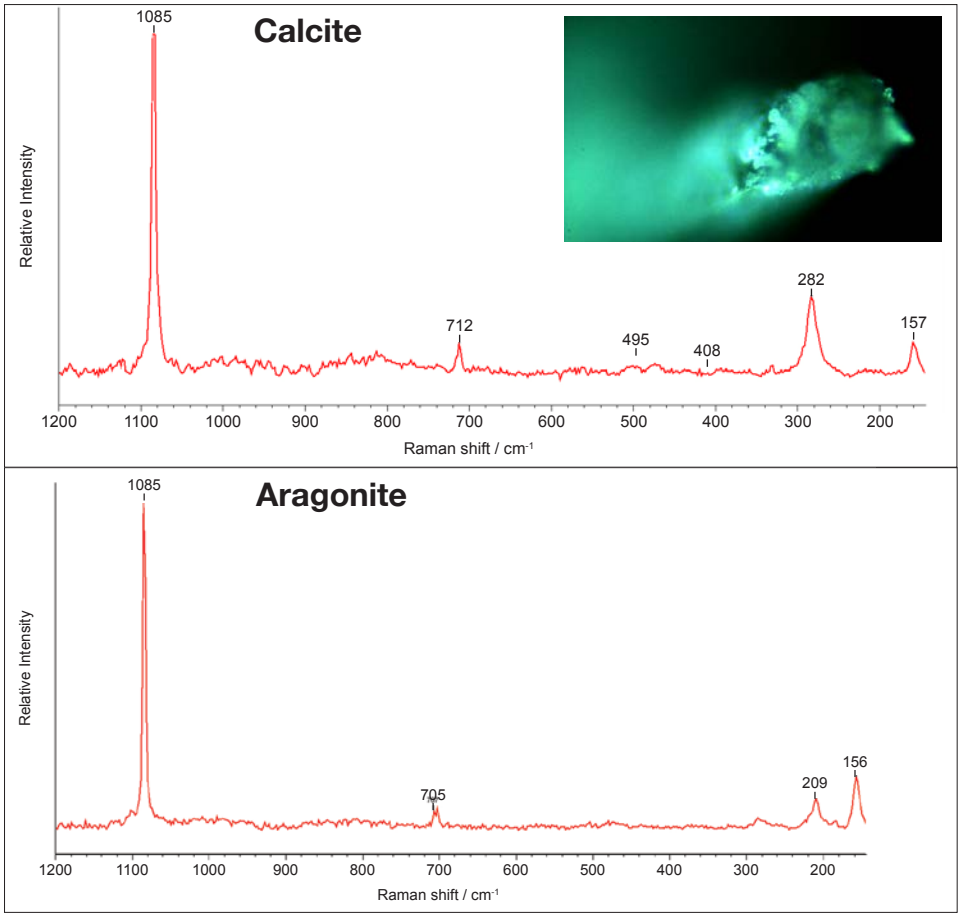

Figure 20a-b. Raman spectra obtained focusing the laser source on small particle inclusions. It is possible to obtain the characteristic bands of the calcite (157, 282, 712, 1086 cm^{-1}) and aragonite (156, 209, 703 and 707, 1085 cm^{-1}) mineral phases.

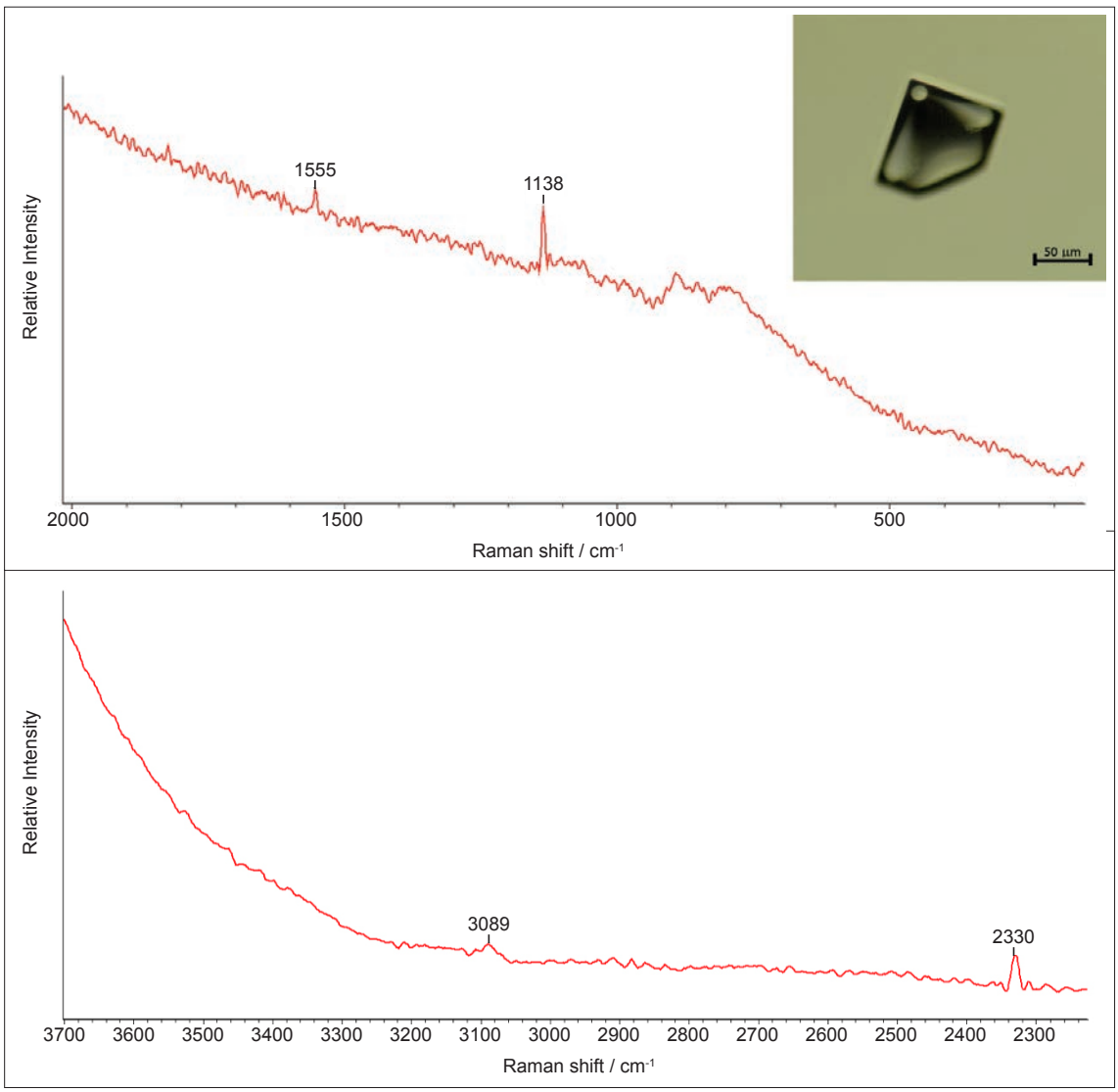

Figure 20c-d. Raman spectrum obtained from the fluid inclusion reported as microscopy image in the box, (a) and (b) are the low and high spectroscopy range, respectively. The sharp aspect of the bands suggests a gaseous origin for the Raman scattering. The band at 1555 cm^{-1} could be correlated with the molecular oxygen vibrational mode *(Socrates, 2001)*. The band at 1138 cm^{-1} is in the spectroscopy range correlated to typical carbonium vibrational mode, as well as the band at 3089 cm^{-1} is characteristic for CH stretching; in fact, Larkin (2011) reports the band at 1138 cm^{-1} as a very strong mode of furan ring. The band at 2330 cm^{-1} is typical for molecular nitrogen vibrational *(Dubessy, 1989; Socrates, 2001)*. No CO_2 bands at 1385 and 1278 cm^{-1}, as reported for Fermi CO_2 resonance doublet *(Dubessy, 1989; Larkin, 2011)*, and no 2522 cm^{-1} correlated to H_2S *(Dubessy, 1989)* are detected.

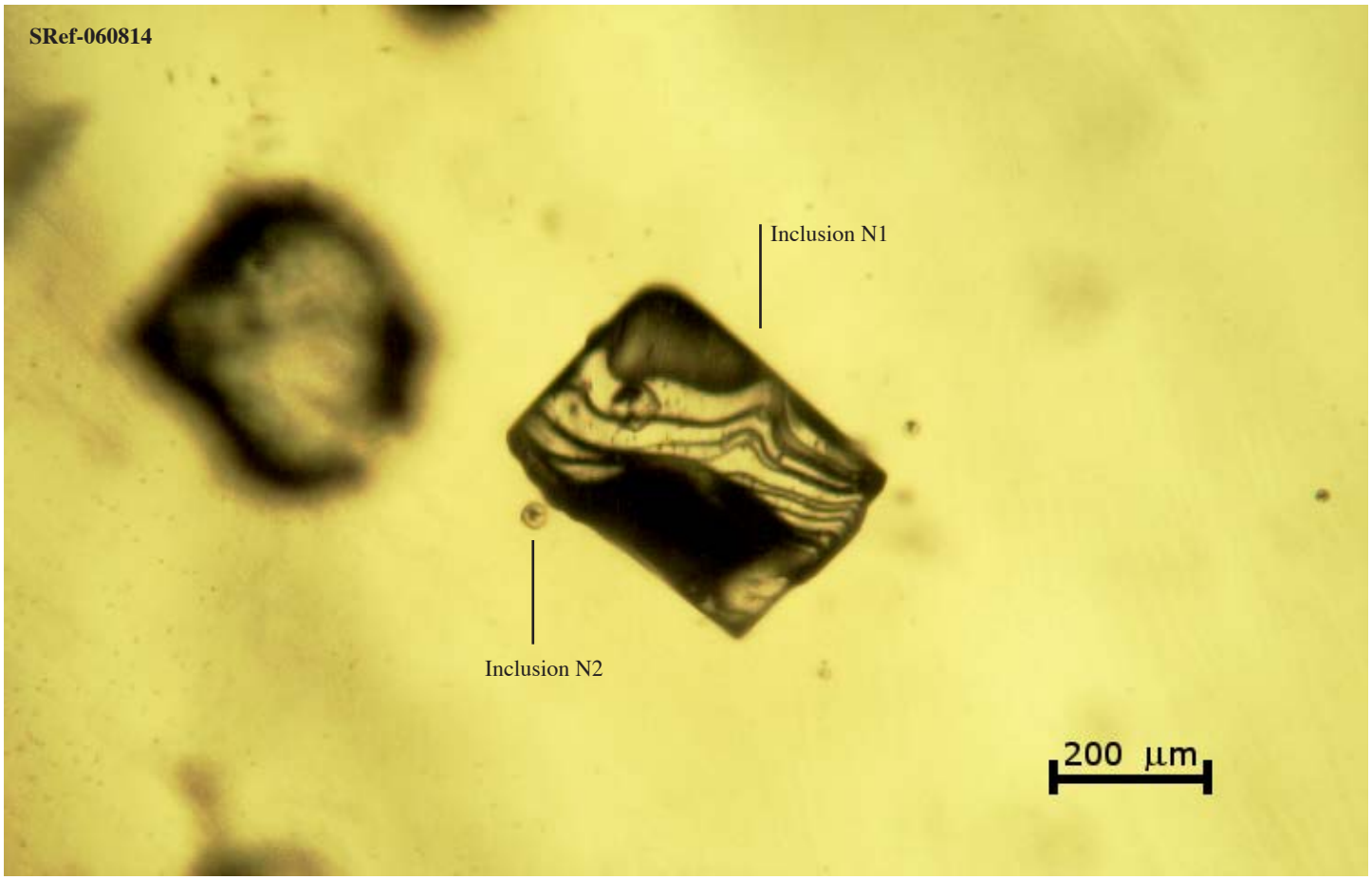

Figure 21a-c. Microscopic image of several inclusions observed in the samples using transmitted light, which reveal different shapes and surface details. The large rectangular inclusion has no Raman bands in the spectrum.

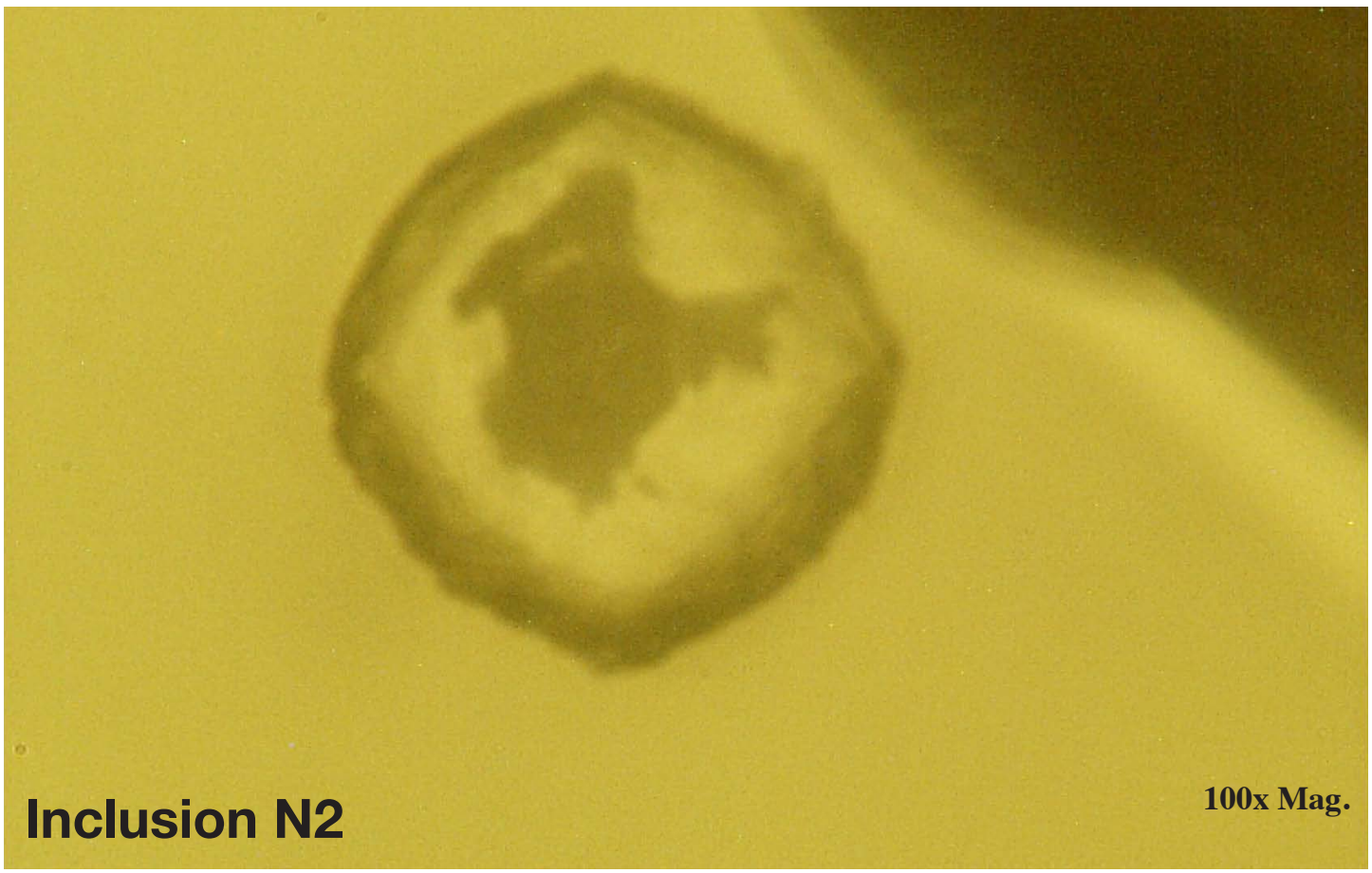

Figure 21b.

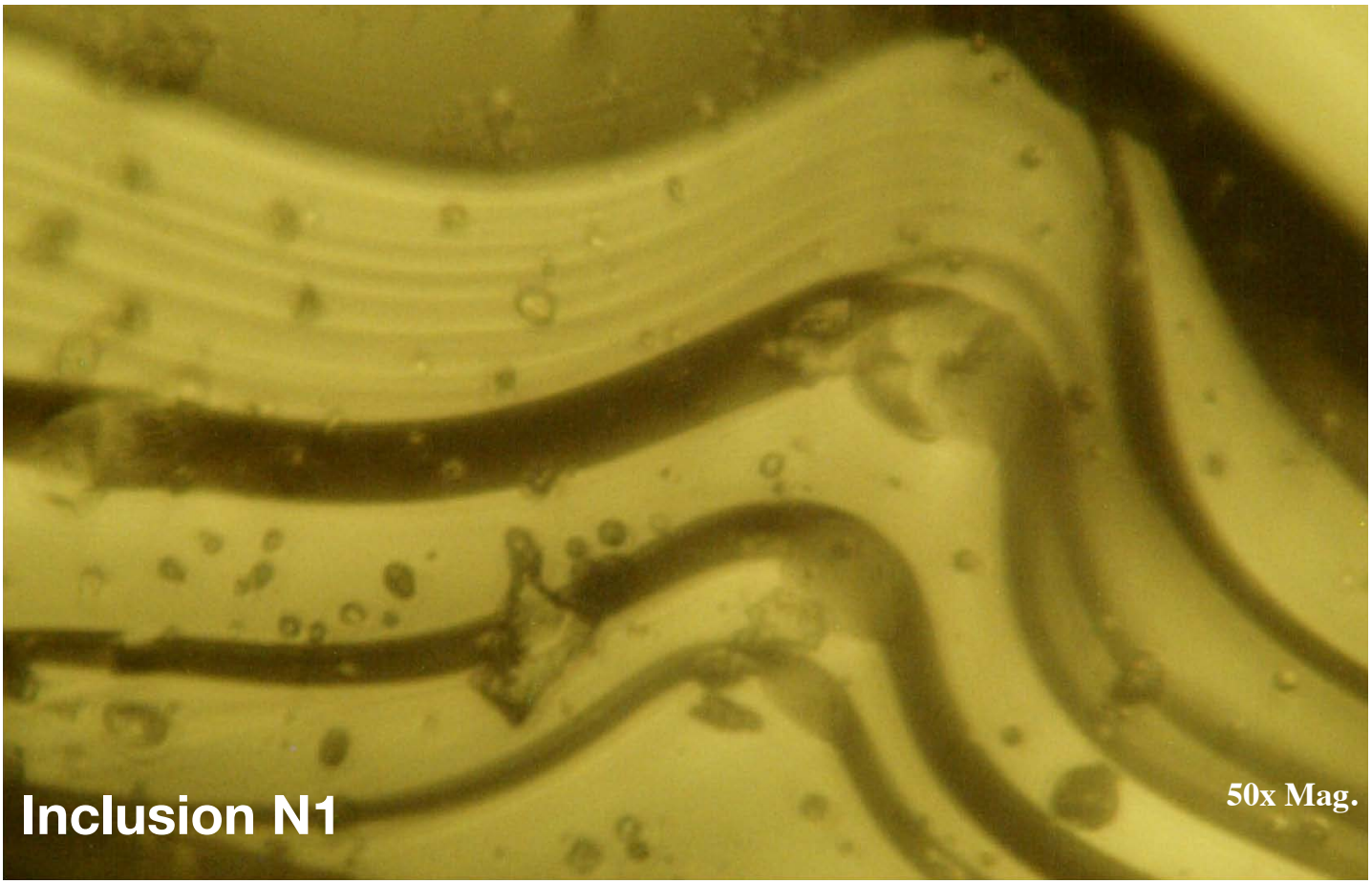

Figure 21c.

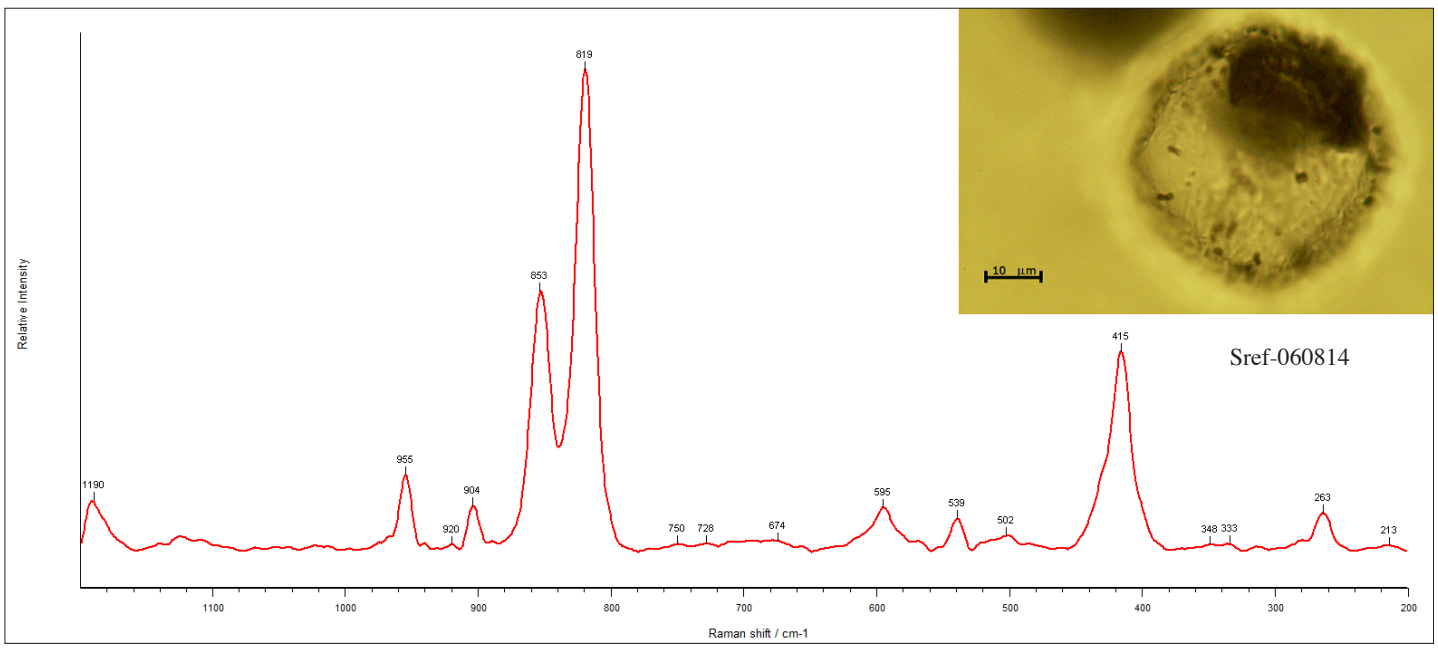

Figure 21d. Raman spectrum of the samples spherical inclusions *(see inserted picture)*. The main bands at 263, 415, 539, 595, 819, 853, 904 and 955 cm^{-1} are compatible with olivine phases of the forsterite-monticellite series.

Discussion

The positive identification of synthetic periclase was possible by solid inclusion analysis. A Ca-Si-oxide inclusion was identified as a cement hardener C_2S (dicalcium silicate). As reported by Ibanez et al. (2007) and Ramirez & Carrasco (2011), this is an artificial compound and it represents a typical Portland cement synthetic product.

Other inclusions contained unknown chemical compositions, such Fe-P bearing particles that were found by SEM-analysis. We are not aware of equivalent minerals existing in nature with such a chemical composition.

We identified minerals of the monticellite-forsterite series (synthetic or natural) showing an unusual skeletal radiating growth. We did not find equivalent natural minerals in the literature with this kind of growth feature. In cavities, we found hematite phases, nano-particles of aragonite in association with calcite, but no hydrated phases. Some of these inclusions have natural equivalents (calcite, aragonite, hematite) but are still found together with synthetic C_2S. Therefore, they are also of synthetic nature.

A phosphorous bearing black inclusion lacking Mg, Ca and Si was interpreted as a "rubber" slag particle. It was found included inside the periclase after the rough periclase material was broken up. It is most probably an accidental contamination during the synthetic production process.

In nature periclase often reacts under the influence of water provided in circulating fluids to form brucite *(Deer, et al., 1994)*. No brucite (a water-bearing mineral) was observed in our analyses. This is consistent to the fact that this periclase was not subjected to natural fluids. Fluid inclusion analysis showed the absence of CO_2-bearing fluids. Thus the idea that periclase is formed in a natural process involving decarbonatization processes (with formation of CO_2) can be rejected *(see discussion in the introduction)*.

The inter-growth of the solid materials as seen in SEM-EDS scanning analysis shows a pattern reminiscent of eutectic formation *(see flame structures in Fig. 12a)*. Such textures may well indicate formation from high-temperature oxide melts such as in the system CaO-MgO-SiO_2. Thermodynamic phase diagrams of melted oxides (slags) in the system SiO_2-MgO-CaO have been published by Jung et al. (2004). The diagram shows that a variety of minerals can be formed from such oxide melts by cooling *(Fig. 23)*. This can explain the occurrence of calcium-silicate minerals and monticellite-forsterite minerals in our synthetic periclase.

As shown in Fig. 22, depending on the starting chemical composition, MgO rich melts will form periclase. When the chemical composition is variable with additional SiO_2 or CaO, a series of other minerals can be formed from these oxide melts. From these components the synthetic formation of forsterite-monticelllite can be formed along a cooling path together with periclase. Other solid materials with different Ca/Si-ratios can be formed in the system CaO-SiO_2 as well.

Our samples contained isolated areas with many inclusions. These areas are interpreted as chemically inhomogeneous melts that are formed in the production process. From these contaminated melts, occasionally C_2S and monticellite-forsterite was formed.

Conclusion

In this article we have presented the gemological properties, fluorescence behaviors using DiamondView *(Fig. 10, page 8)*, UV-VIS-NIR spectroscopy *(Fig.9a-d, page 7)*, Raman spectra *(Appendix A, page 28)*, photoluminescence *(Appendix D, page 31)* and FTIR spectra *(Appendix B, page 29)* as well as the chemical composition measured with LA-ICP-MS *(Appendix C, page 30)* of various colors of synthetic periclase.

The identification of these new synthetics of different colors would not have been possible without sophisticated inclusion analysis. It was critical that rough material was available that allowed a specific targeting of selected areas and inclusion for investigation. Additional investigation methods allowed us to further characterize these synthetic periclase and provide the results as fingerprint data for the gemological community. It is not to be expected that a natural periclase will exactly duplicate the spectroscopic features and chemical compositions, including minor and trace elements of these synthetic periclase.

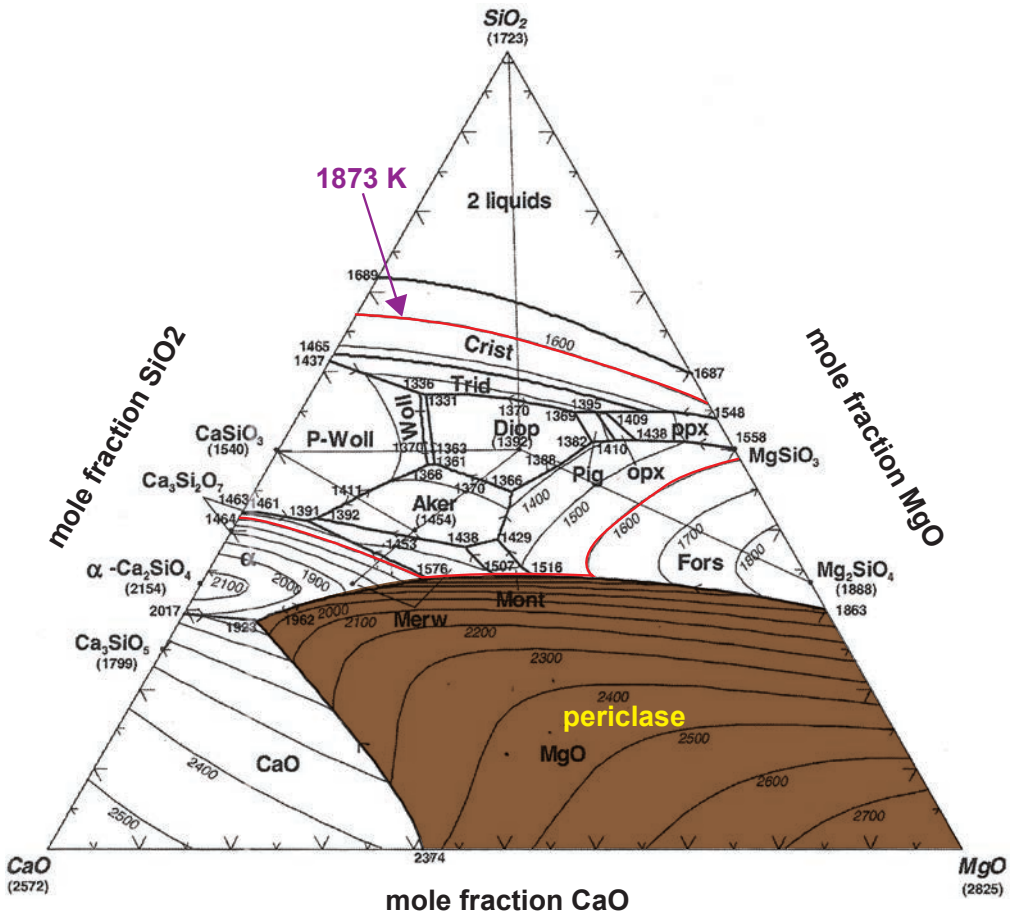

Legend	
Crist	Cristobalite
Trid	Tridimite
P-Woll	Ps-Wollastonite
Woll	Wollastonite
Diop	Diopside
opx	Pyroxene
Aker	Akermanite
Merw	Merwinite
Mont	Monticellite
Fors	Forsterite

Figure 22. Calculated (optimized) liquidus surface of the CaO-MgO-SiO_2 system at 1 bar pressure. Temperatures in degree Celsius *(from Jung et al., 2004)*. The diagram shows contours of temperatures and stability of solid materials. During cooling, synthetic materials will be formed depending on the initial composition of the melts. Field for synthetic periclase is shown in color. For other synthetic materials see Legend.

References

R.T. Liddicoat, Synthetics examined, Gems & Gemology. 1969; 13, 22;

G. Brown, Australian synthetic Periclase, The Australian Gemmologist, Vol.18, N.8, 1993;

K. K. Chow, M. Short, S. Lam, A. McWilliams, and H. Zeng, A Raman cell based on hollow core photonic crystal fiber for human breath analysis, Medical Physics 41, 2014;

W.A. Deer, R.A., Howie, J. Zussman, in: Zanichelli (Ed.) Introduzione ai minerali che costituiscono le rocce 2nd ed., Bologna, 1994;

M. De Maggio & SFM, Synthetic Green Periclase, lab notes, Gems & Gemology, Fall 1997;

K. Dück, B. W. Rawe, M. R. Scott, D. P. Gates, Polymerization of 1-Phosphaisoprene: Synthesis and Characterization of a Chemically Functional Phosphorus Version of Natural Rubber, Angew. Chem. Int. Ed. 2017, 56, 9507.

J. Dubessy, B. Poty and C. Ramboz, Advances in C-O-H-N-S fluid geochemistry based on micro-Raman spectrometric analysis of fluid inclusions, European Journal of Mineralogy, 1, 517-534, 1989.

Farmer, V. C., Infrared spectra of minerals, Mineralogical Society of Great Britain and Ireland, 1974;

B. Joachim, A. Wohlers, N. Norberg, E. Gardes, E. Petrishcheva, R. Abart, Diffusion and solubility of hydrogen and water in periclase, Phys Chem Minerals, 2012;

Jordi Ibanez, Luıs Artus, Ramon Cusco, Angel Lopez, Esperanza Menendez and Marıa C. Andrade, Hydration and carbonation of monoclinic C_2S and C_3S studied by Raman spectroscopy, J. Raman Spectrosc. 2007; 38: 61–67;

In-Ho Jung, Sergei A. Decterov, Arthur D. Pelton, Critical Thermodynamic Evaluation and Optimization of the CaO-MgO-SiO_2 System, Journal of Phase Equilibria and Diffusion, 2005 25(4):313-333;
P. Larkin, Infrared and Raman Spectroscopy principles and spectral interpretation, Elsevier, 2011;

S.G. Marchetti, R. Spretz, M.A. Ulla and E.A. Lombardo, Identification of the species formed in the Fe/MgO system: A Raman and Mössbauer study, Hyperfine Interactions 128 (2000) 453–466 453;

K. Mohanan & S. K. Sharma, A Raman spectral study of forsterite-monticellite solid solutions, American Mineralogist, Volume 78, pages 42-48, 1993;

Sir C.V. Raman, The vibration spectra of crystals-Part IV Magnesium oxide, Proc. Indian Acad. Sci. A26 383-390 (1947);

S. M. Ramirez & L. F. Carrasco, Raman Spectroscopy: application of cementizious systems, in: construction and building: design, materials and techniques, 2011;

G. Socrates, Infrared and Raman Characteristic Group Frequencies - Tables and Charts, III Ed., John Wiley & Sons, 2001.

M. Scott, [website] www.rruff.info, S100407, Larnite R070530.

Appendix A

Raman spectra of SRef-060812 synthetic periclase measured by different lasers and measuring conditions

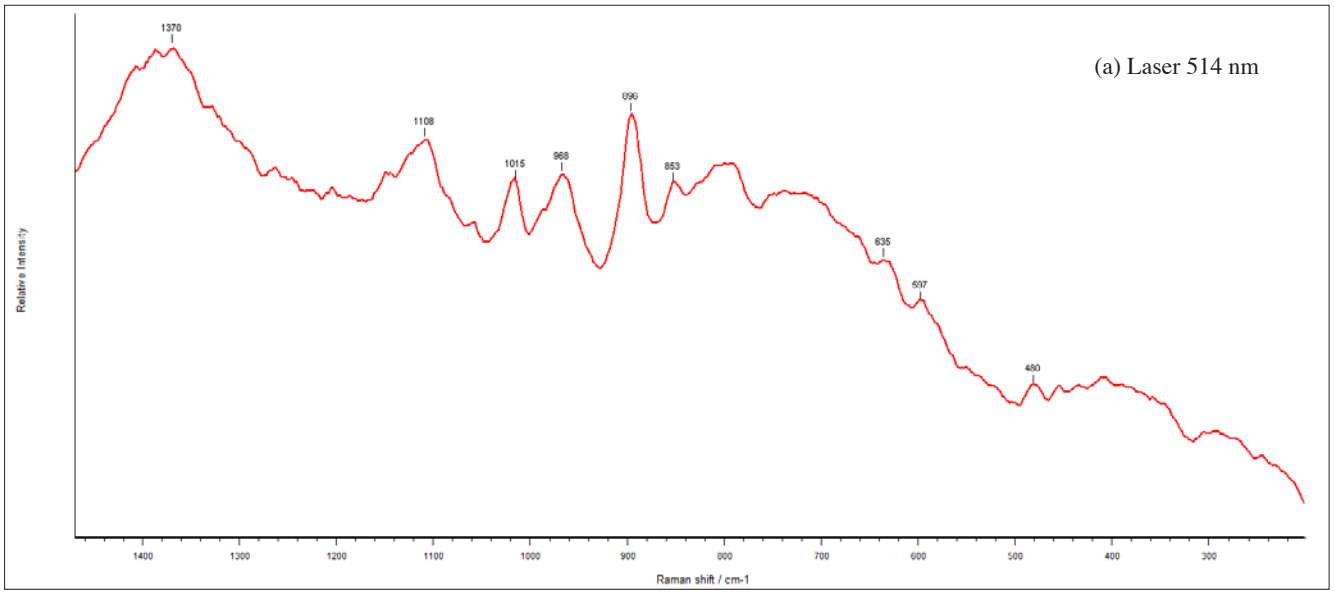

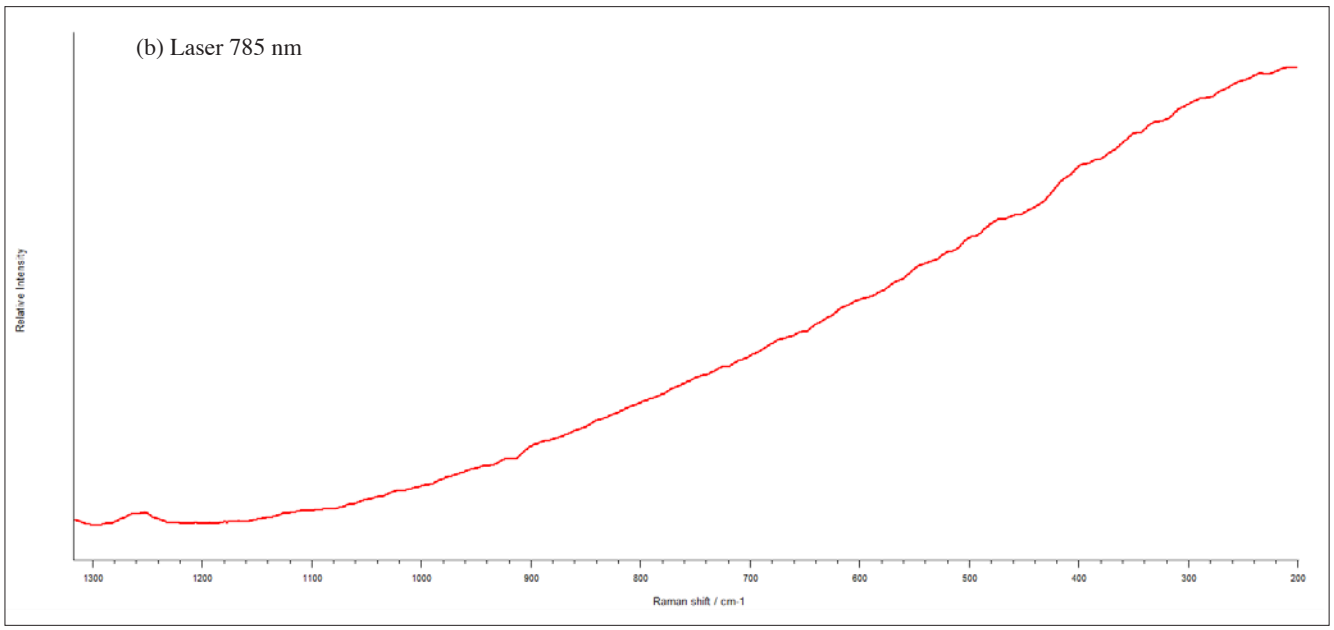

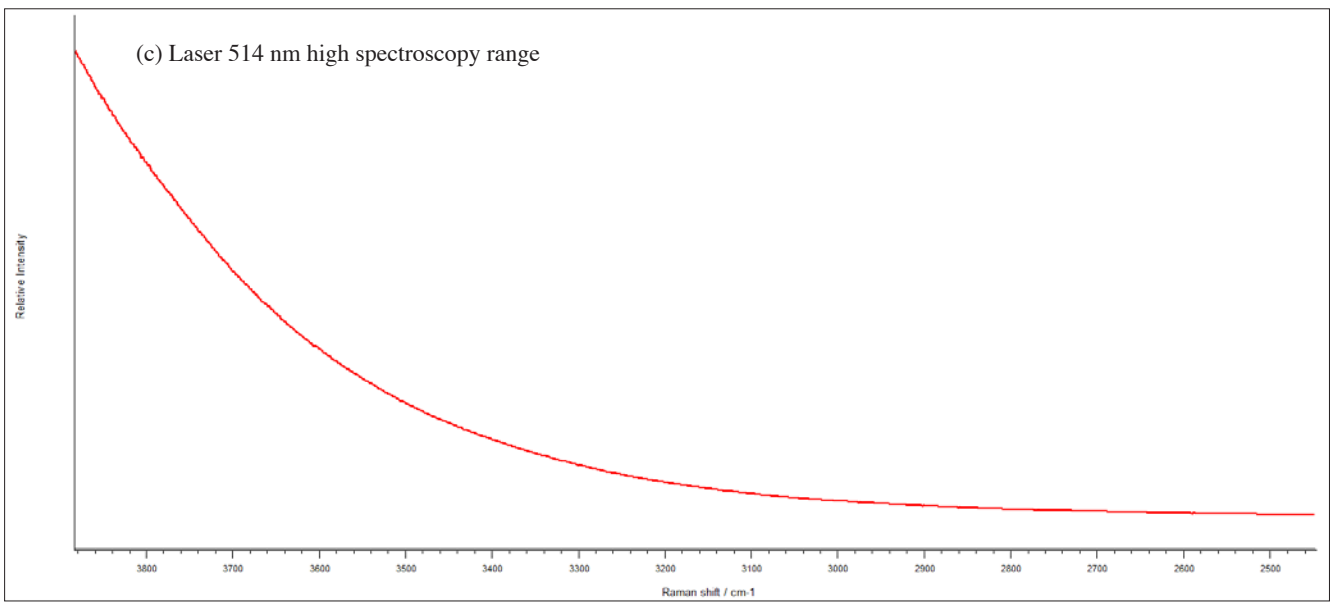

Raman characterization of the bulk crystals, spectra acquired focusing the laser source on the samples surface. **(a)** 514 nm source, low spectroscopy range; **(b)** 785 nm source same spectroscopy range of **(a)** and **(c)** 514 nm source, high spectroscopy range. SRef-060812.

Appendix B

FTIR spectra of same synthetic periclase measured by different FTIR and measuring conditions

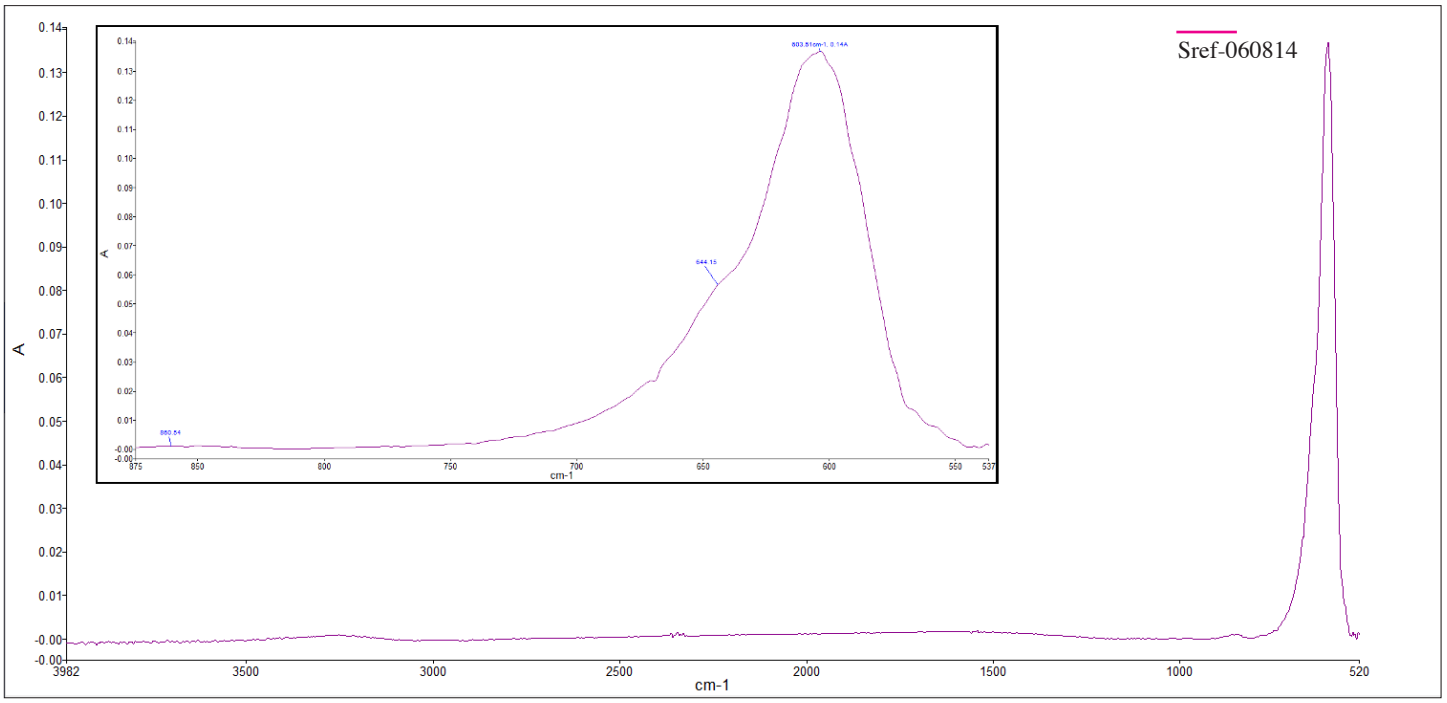

FTIR absorption spectrum acquired by the ATR crystal applied on the surface of the synthetic periclase. In all the samples are well visible very faint and broad bands at about 3300, 850 cm^{-1} and a strong band at about 603 cm^{-1}. Thanks to the application of a fitting program, a second band is also visible at about 645 cm^{-1}, as reported in the box.

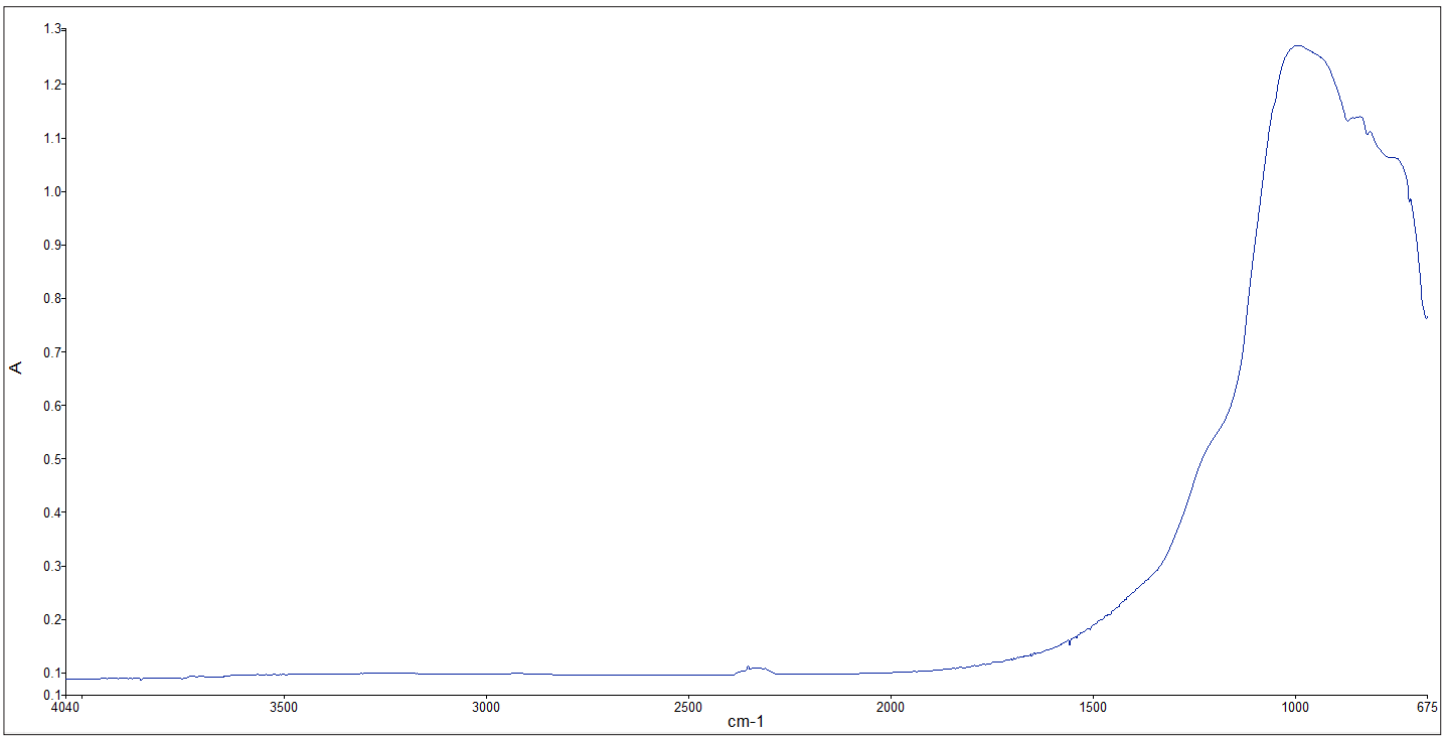

IR absorption spectrum acquired by micro-FTIR instrument in bulk transmission mode on the synthetic periclase. The fingerprint spectroscopy range results saturated, as expected for gemstones analyses, and no other characteristic band has been registered.

Appendix C

Results LA-ICP-MS

The data show a chemical composition dominated by MgO with minor elements including SiO_2 and CaO. Trace elements include elevated Cr, Mn and Fe-concentrations for the green sample. Ni, Cu and Zn-concentrations are found in both samples. No concentrations of REE elements and no concentrations of a variety of elements are found above detection levels *(see table 2)*.

Table 2. LA-ICP-MS data of synthetic periclase

	SRef-60811 Synthetic green Periclase			SRef-60814 Synthetic orange Periclase			
	Spot 1	**Spot 2**	**Spot 3**	**Spot 1**	**Spot 2**	**Spot 3**	**Mean LOD [ppm]**
Wt%-of-oxide							
MgO	99.6	99.6	99.7	99.5	99.7	99.7	40
SiO_2	0.1	0.09	0.08	0.14	0.1	0.1	80
CaO	0.23	0.19	0.17	0.13	0.11	0.09	50
Trace elements ppm							
S	<LOD	170	<LOD	410	<LOD	<LOD	130
Cl	36	48	39	64	50	58	24
Ti	<LOD	1.2	2.2	<LOD	<LOD	<LOD	1.0
V	1.04	0.99	0.86	0.16	<LOD	0.13	0.11
Cr	290	262	216	26.1	23.1	21.7	1.0
Mn	38.2	33.9	28.0	133.0	123.0	111.0	0.2
Fe	407	363	295	778	662	582	17
Ni	15.5	15.1	12.4	16.1	14.0	11.9	0.4
Cu	1.6	1.6	1.4	2.6	2.0	2.0	0.6
Zn	4.9	4.4	3.4	8.7	5.4	4.6	1.6

The following elements were detected by LA-ICP-MS analysis as concentrations in the range of ppm levels: S, Cl, Ti, V, Cr, Mn, Fe, Ni, Cu, Zn and a series of elements were below the limits of detection "LOD" (with corresponding detection limits in ppm): Li(0.3), Be(0.4), B(2), Na(10), Al(10), K(2), Sc(0.4), Co(1.5), Ga(0.2), Ge(0.5), As(0.5), Mo*, Sn*, Cs(0.1), Ba*, La*, Ce*, Pr*, Nd*, Eu*, Gd*, Tb*, Dy*, Ho*, Er*, Tm*, Yb*, Lu*, Hf*, W*, Pt*, Au*, Pb*, Bi*, Th*, U*

* the concentration could not be determined. The median of the signal (background and sample signal) is equal or < 0 cps.

Appendix D

Photoluminescence of synthetic periclase

All different colors of synthetic periclase showed distinctive peaks. Photoluminescence spectra were varying for the different colors, mainly in the intensity of the different emission lines. According to our knowledge these are the only and first photoluminescence spectra of synthetic periclase in the literature. A comparison with natural periclase is in progress at the time of the release of this study.

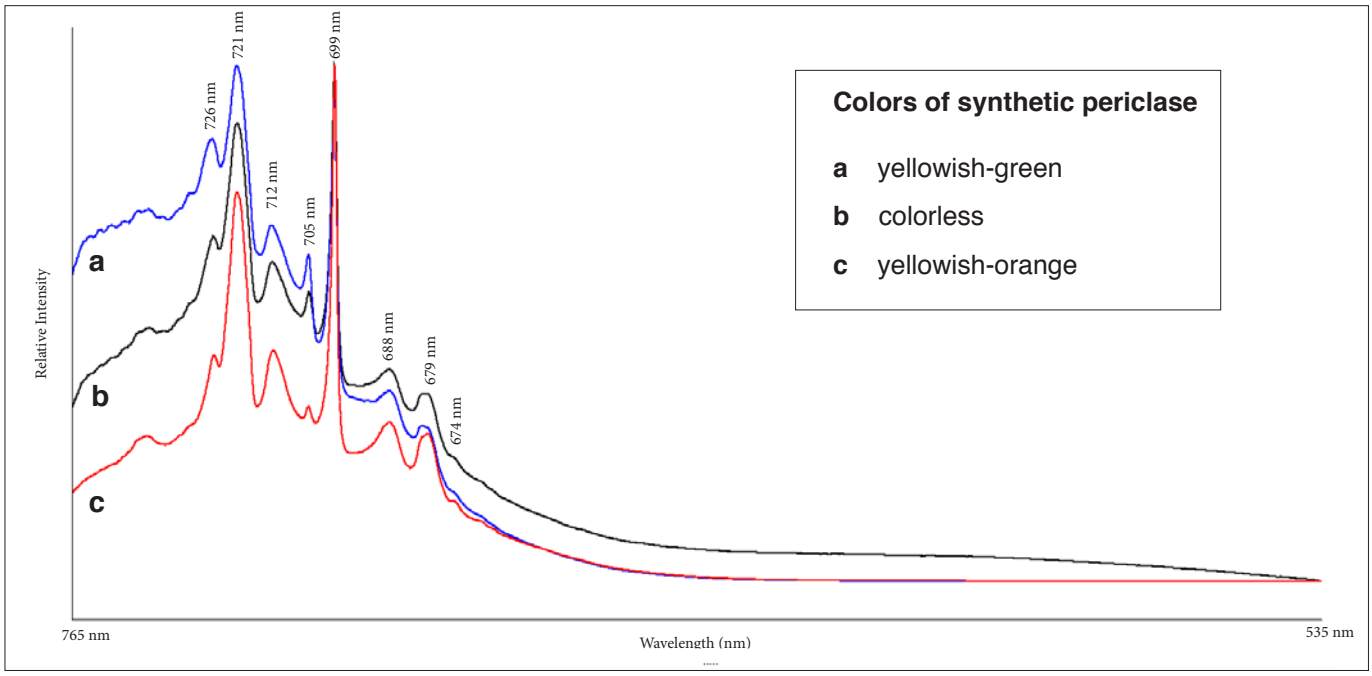

Photoluminescence spectra of three different colors of synthetic periclase. Colorless *(black line)*, yellowish-green *(blue line)* and yellowish-orange *(red line)*.